



HAL
open science

Unveiling African rainforest composition and vulnerability to global change

M. Réjou-Méchain, Frédéric Mortier, Jean-François Bastin, Guillaume Cornu, Nicolas Barbier, Nicolas Bayol, Fabrice Bénédet, Xavier Bry, Gilles Dauby, Vincent Deblauwe, et al.

► To cite this version:

M. Réjou-Méchain, Frédéric Mortier, Jean-François Bastin, Guillaume Cornu, Nicolas Barbier, et al.. Unveiling African rainforest composition and vulnerability to global change. *Nature*, 2021, 593, pp.90-94. 10.1038/s41586-021-03483-6 . hal-03205277

HAL Id: hal-03205277

<https://hal.inrae.fr/hal-03205277v1>

Submitted on 21 Oct 2021

HAL is a multi-disciplinary open access archive for the deposit and dissemination of scientific research documents, whether they are published or not. The documents may come from teaching and research institutions in France or abroad, or from public or private research centers.

L'archive ouverte pluridisciplinaire **HAL**, est destinée au dépôt et à la diffusion de documents scientifiques de niveau recherche, publiés ou non, émanant des établissements d'enseignement et de recherche français ou étrangers, des laboratoires publics ou privés.

1 **Title: Unveiling African rainforest composition and vulnerability to global change**

2 **Authors:** Maxime Réjou-Méchain^{1*}, Frédéric Mortier^{2,3}, Jean-François Bastin^{1,2,3,4},
3 Guillaume Cornu^{2,3}, Nicolas Barbier¹, Nicolas Bayol⁵, Fabrice Bénédet^{2,3}, Xavier Bry⁶,
4 Gilles Dauby¹, Vincent Deblauwe^{7,8}, Jean-Louis Doucet⁹, Charles Doumenge^{2,3}, Adeline
5 Fayolle⁹, Claude Garcia^{2,3,10}, Jean-Paul Kibambe^{11,12}, Jean-Joël Loumeto¹³, Alfred
6 Ngomanda¹⁴, Pierre Ploton¹, Bonaventure Sonké¹⁵, Catherine Trottier⁶, Ruppert Vimal¹⁶,
7 Olga Yongo¹⁷, Raphaël Pélissier¹, Sylvie Gourlet-Fleury^{2,3}

8 **Affiliations:**

- 9 1. AMAP, Univ Montpellier, IRD, CNRS, CIRAD, INRA, Montpellier, France.
- 10 2. CIRAD, Forêts et Sociétés, F-34398 Montpellier, France.
- 11 3. Forêts et Sociétés, Univ Montpellier, CIRAD, Montpellier, France.
- 12 4. Crowther Lab, Department of Environmental Systems Science, Institute of
13 Integrative Biology, ETH Zürich, Zürich, Switzerland.
- 14 5. Foret Ressources Management Ingénierie, 34130 Mauguio – Grand Montpellier,
15 France.
- 16 6. Institut Montpelliérain Alexander Grothendieck (IMAG), Montpellier, France.
- 17 7. Center for Tropical Research, Institute of the Environment and Sustainability,
18 University of California, Los Angeles, Los Angeles, CA 90095, USA.
- 19 8. International Institute of Tropical Agriculture, Yaounde, Cameroun.
- 20 9. Université de Liège, Gembloux Agro-Bio Tech, Forest is Life, TERRA Teaching and
21 Research Centre, Passage des Déportés 2, 5030 Gembloux, Belgium.
- 22 10. Forest Management and Development Team, Department of Environmental
23 System Science, Institute of Integrative Biology, ETH Zürich, Zürich, Switzerland.
- 24 11. Faculté des Sciences Agronomiques, Département de Gestion des Ressources
25 Naturelles, Université de Kinshasa, Kinshasa I, Democratic Republic of Congo.
- 26 12. Wildlife Conservation Society, Kinshasa, Congo, Democratic Republic of Congo.

- 27 13. Faculté des Sciences et Techniques, Université Marien Ngouabi, BP 69
28 Brazzaville, Republic of Congo.
- 29 14. Institut de Recherche en Ecologie Tropicale (IRET/CENAREST), B.P. 13354
30 Libreville, Gabon.
- 31 15. Plant Systematic and Ecology Laboratory, Higher Teacher's Training College,
32 University of Yaoundé I, Yaoundé, Cameroon.
- 33 16. GEODE UMR 5602, CNRS, Université Jean-Jaurès, 5 Allée Antonio-Machado,
34 Toulouse, France.
- 35 17. Laboratoire de Biodiversité Végétale et Fongique, Faculté des Sciences, Université
36 de Bangui, Bangui, Central African Republic.
- 37

38 **Africa is forecasted to experience large and rapid climate change¹ and population**
39 **growth² during the XXIst century, threatening the world's second largest**
40 **rainforest. Protecting and sustainably managing these forests requires an**
41 **extended understanding of their current compositional heterogeneity,**
42 **environmental drivers and vulnerability to ongoing changes. Here, using an**
43 **unprecedented dataset of 6 million trees in more than 180,000 field plots, we**
44 **jointly model the distribution in abundance of the most dominant central African**
45 **tree taxa and produce the first continuous maps of the floristic and functional**
46 **composition of central African forests. Our results show that the uncertainty in**
47 **taxon-specific distributions averages out at the community level, revealing highly**
48 **deterministic assemblages. We uncover contrasting floristic and functional**
49 **compositions across climate, soil types and anthropogenic gradients, with**
50 **functional convergence among floristically dissimilar forest types. Combining**
51 **these spatial predictions with global change scenarios suggests a high**
52 **vulnerability of the northern and southern forest margins, the Atlantic forests and**
53 **of most forests from the Democratic Republic of Congo where both climate and**
54 **anthropogenic threats are expected to increase sharply by 2085. These results**
55 **constitute key quantitative benchmarks for scientists and policy makers to shape**
56 **transnational conservation and management strategies aiming at providing a**
57 **sustainable future for central African forests.**

58 Concomitant increases in climate stress, human population needs and resource
59 extraction in central Africa raise environmental concerns³⁻⁵. These threats may have
60 considerable impacts on the carbon budget⁶, climate⁷ and biodiversity of central African
61 forests⁸, which shelter some of the world's most iconic wildlife species and that are
62 already experiencing much drier and seasonal climate than other tropical forests⁹.
63 However, the current composition of central African forests and its determinants at
64 regional scale are still poorly known, being often studied on limited areas¹⁰⁻¹² and
65 datasets¹³ or at a very coarse grain with heterogeneous presence-only data¹⁴. Vast
66 areas remain poorly scientifically explored¹⁵ while most spaceborne systems of Earth

67 observation provide very limited information on forest composition¹⁶. This limits our
68 ability to understand how forest composition and functions vary regionally, to forecast
69 how these forests will face upcoming global changes and, ultimately, to anticipate, on
70 scientific bases, how to protect and manage them beyond national boundaries.

71 In this study, we used an unprecedented forest inventory dataset to (1) model the main
72 floristic and functional gradients over central African forests, and (2) assess their
73 expected vulnerability under forecasted global (climatic and anthropogenic) change
74 conditions. We compiled the abundance distributions of 193 dominant tree taxa in
75 185,665 field plots (ca. 90,000 ha) from commercial forest inventories spread over the
76 five main forested countries in central Africa (Extended Data Fig. 1). We modeled the
77 joint distributions of taxon abundances at a 10-km resolution using supervised
78 component generalized linear regression (SCGLR)¹⁷, a modelling method that extends
79 partial least squares (PLS) regression to the multivariate generalized linear framework.
80 SCGLR models a set of responses (here the abundances of taxa) from synthetic
81 orthogonal explanatory components derived from 24 climatic variables (hereafter,
82 climatic components, CCs) and additional soil type (here, sand vs. clay) and
83 anthropogenic pressure covariates. We developed for this study an index based on
84 population density and road network specifically designed and calibrated to predict
85 recent human-induced forest disturbance intensity in central Africa - see Methods.
86 Finally, thanks to the huge size of the dataset, the predicted floristic and functional
87 gradients were cross-validated with spatially independent observations using Spearman
88 correlation coefficients, ρ_{CV} .

89 **Floristic composition in central Africa**

90 Our model predicted individual taxon abundances with an overall median correlation ρ_{CV}
91 of 0.48 (range of -0.11 to 0.83). This median was still as high as 0.45 when unoccupied
92 sites were removed, showing that, beyond presence-absence, our model also captured
93 variations in abundances within taxon's distributional range. A correspondence analysis
94 (CA) performed on the predicted taxon abundances revealed major regional floristic
95 gradients (Fig. 1; Extended Data Fig. 2 and 3) highly correlated with the observed

96 gradients ($\rho_{CV}=0.89, 0.71$ and 0.6 for CA axes 1 to 3, respectively; Fig. 1B-D). Contrary
97 to Amazonian and Southeast Asian forests, where soil was shown to be the primary
98 large scale driver of tree community composition^{18,19}, the most prominent floristic
99 gradient predicted here (CA axis 1) was highly related to climate, in particular to the first
100 predictive CC (Pearson's $r=0.98$), contrasting areas with a cool and light-deficient²⁰ dry
101 season (coastal Gabon) and areas with high evapotranspiration rates (northern limit of
102 the central African forests; Extended Data Fig. 4). The second predicted floristic
103 gradient (CA axis 2) was highly correlated with the two other CCs ($r=-0.86$ and -0.72 for
104 CC2 and CC3, respectively) related to seasonality and maximum temperature, thus
105 contrasting equatorial areas with a low water deficit and areas with a high water deficit
106 towards the limits of the tropics. Climate seasonality was also found to be an important
107 driver of tree community composition in Amazonia¹⁸ and maximum temperature has
108 been recently identified as the most important pantropical driver of forest biomass,
109 impacting woody productivity²¹. The third predicted floristic gradient (CA axis 3) revealed
110 more local floristic variations highlighting human-impacted forests ($r=0.67$ with our index
111 of human-induced forest disturbance intensity).

112 As already shown in previous studies^{22,23}, the association between taxon distributions
113 and climate patterns may appear by chance because both are spatially autocorrelated
114 at the regional scale. We thus used a spatially explicit null model that randomized the
115 predictive CCs while preserving their spatial (co)structures. When keeping the soil and
116 human impact on forests unchanged, the null model did not predict significantly different
117 abundances ($P>0.1$) from those predicted with original CCs for 67% of the taxa. This
118 suggests that variation in taxon abundances directly depends on climate for a minimum
119 of only one-third of the taxa, while for most of them, abundance may correlate with
120 climate by chance only. In contrast, the association between climate and the main
121 gradients of floristic assemblages was robust to autocorrelation artifacts ($P=0.028$,
122 0.006 and 0.06 for CA1 to 3, respectively). This result confirms that extrapolating
123 assemblages from climate variables is more reliable than extrapolating individual taxon
124 abundances²⁴. Indeed, individual taxon abundances are likely less predictable on the

125 basis of only current drivers since they are also affected by unknown past human
126 disturbances²⁵, biotic interactions and biogeographical history²⁶, the idiosyncratic effects
127 of which tend to average out at the community level.

128 **Functional composition in central Africa**

129 From the predicted floristic assemblages, we computed the community weighted mean²⁷
130 of three functional traits known to play an important role in ecosystem processes: wood
131 density, deciduousness and maximum diameter (Fig. 2). The predicted functional
132 composition was consistent with the observations (ρ_{CV} =0.47, 0.75 and 0.45 for the three
133 traits, respectively; Extended Data Fig. 5). As in Amazonia¹⁸, community wood density
134 varies with soil type with the highest values found on sandy soils, at the boundaries of
135 Cameroon, Republic of Congo and Central African Republic, where tree species with
136 conservative resource use strategies predominate¹¹. However, larger scale variations in
137 wood density were primarily driven by human-induced forest disturbances, with a lower
138 community wood density in human-impacted forests, indicating that they are mostly
139 composed of fast-growing taxa²⁸. However, these areas also feature a high proportion of
140 trees that can potentially reach a large diameter. These two results indicate that human-
141 impacted forests are dominated by long-lived pioneer taxa, which are characterized by a
142 low wood density but a large potential stature, offering a fast and relatively long-lasting
143 carbon sink potential in absence of disturbances²⁹. Finally, a marked deciduousness
144 gradient ran from the highly evergreen forests of coastal Gabon to the northern limit of
145 the central African forests with, again, a well-known exception on the northern sandy
146 soil plateau^{11,30}.

147 **A reference map of forest types**

148 To ease practical applications, we performed hierarchical clustering of the predicted
149 floristic gradients (pixel scores on the first five CA axes), which are continuous by
150 nature, and identified ten major forest types (Fig. 3; Extended Data Table 1). The
151 strongest floristic dissimilarity appeared between Atlantic forests (types 1 to 3) and the
152 other forest types (4 to 10), within which semideciduous seasonal forests were clearly

153 distinguished (types 4 to 6). We also observed functional convergences among
154 floristically dissimilar forest types and vice versa. For example, despite having a
155 regional species pool similar to deciduous forests (types 4 and 6), sandstone forests
156 (type 5) have a functional composition closer to remote forest groups (e.g. types 2, 3, 7
157 and 8), with high wood density and low deciduousness. Soil filtering indeed modifies the
158 relative abundance of species (rather than their presence or absence³¹) favoring
159 suitable functional attributes in poor sandy soils¹¹. By contrast, while Atlantic forests
160 (types 1 to 3) have little taxonomic affinity with the east-central and southern forests
161 (types 7 and 8), they display similar functional composition due to more similar climate
162 conditions, as represented on the first predictive CC (Extended Data Table 1). This
163 confirms that while taxonomic composition has an important biogeographical
164 component, the functional composition of tree communities can converge in similar
165 environmental conditions.

166 **Vulnerability to global change**

167 For the ten forest types, most climate models predict current climate conditions either to
168 virtually disappear from central Africa (e.g., types 2 and 5; Extended Data Fig. 6), or to
169 move at spatial and temporal scales incommensurate with tree dispersal ability
170 (e.g. types 4 and 6). This suggests that current forest communities will not be able to
171 track their present climate envelopes and will face the emergence of novel climates,
172 making the prediction of taxon distributions under future climate projection highly risky³².
173 We thus assessed the vulnerability of central African forests to climate change through
174 their sensitivity, exposure, and adaptive capacity, following the recommendation of the
175 IPCC³³.

176 We quantified sensitivity at the community level using the inverse of the current climate
177 niche breadth of taxa (Fig. 4C) and assuming that assemblages dominated by taxa with
178 narrow environmental tolerances will be more vulnerable to upcoming changes³⁴.
179 Sensitivity appeared to be high in coastal Gabon (type 2), where a high level of species
180 endemism exists³⁵ and in the driest northern margin of central African forests. Recent
181 studies consistently showed that drier tropical forests exhibited larger functional

182 changes than wetter forests in response to a long-term drought in west Africa³⁶ and are
183 likely to be more sensitive to global warming²¹. By contrast, forests from the northwest
184 Cameroon displayed a relatively low sensitivity to current climate conditions, probably
185 because these forests are dominated by widespread tree taxa adapted to anthropogenic
186 pressure (Fig. 2). Long-lived pioneers, typical of these human-impacted forests, are also
187 expected to be favored by a possible acceleration in forest dynamics induced by global
188 change^{37,38}.

189 Exposure to climate change was quantified as the extent to which the current climate
190 determinants (CC1 to 3) are expected to change by 2085, using 18 unique bias-
191 corrected climate model combinations (under the IPCC-AR5 RCP 4.5 scenario; see
192 Extended Data Fig. 7 for other scenarios). We found that exposure to climate change
193 was mostly driven by an increase in drought stress and maximum temperature (Fig. S2,
194 see also^{4,39}). The central and east part of central African forests are predicted to be the
195 most exposed, particularly in the south of the Democratic Republic of Congo (DRC)
196 (Fig. 4D). Note, however, that climate change predictions in central Africa are uncertain
197 because meteorological data for model validation are lacking⁴ (Fig. S3).

198 Finally, we assessed the adaptive capacity of tree communities through their
199 evolutionary potential. We first found highly significant niche conservatism along the first
200 two climate components ($P < 0.002$). This indicates that closely related taxa tend to share
201 similar climate niche spaces at the regional scale and suggests that they could be
202 impacted similarly by future climate change. We thus assumed that higher local
203 phylogenetic diversity provides a wider range of potential responses to novel climate
204 conditions⁴⁰, similarly to the insurance hypothesis⁴¹. We thus used the phylogenetical
205 diversity of predicted tree assemblages as a proxy of their adaptive capacity to climate
206 change. Undisturbed semideciduous and transitional forests (types 6 and 10 in Fig. 3)
207 appeared phylogenetically more diverse, thus having higher adaptive capacity, than
208 evergreen forests (Fig. 4E). A recent study in Amazonia⁴² also found a peak of
209 phylogenetic diversity at intermediate precipitation level, where dry- and wet-adapted
210 lineages are mixing. As expected⁴³, we also found that human-impacted areas tended to

211 have a low phylogenetic diversity and hence a lower adaptive capacity to climate
212 change.

213 The resulting vulnerability of tree communities to climate change did not correlate with
214 the expected human impact on forests in 2085 ($\rho = -0.08$), here assessed using country-
215 specific projections of human population (Fig. 4A; Extended Data Fig. 8). Vulnerability to
216 climate change is expected to be higher for communities dominated by hard-wooded
217 taxa ($\rho = 0.46$ with wood density, Table S1). By contrast, forecasted human impact on
218 forests is predicted to be higher in already disturbed communities, i.e., dominated by
219 light-wooded taxa with a large potential size ($\rho = -0.4$ and 0.43 , respectively). However,
220 because we did not account for the appearance of new roads by 2085, we may
221 underestimate the effect of future anthropogenic activities in remote, currently
222 undisturbed forests. Vulnerability to both climate change and anthropogenic activities
223 (pink color in Fig. 4A) is predicted to be high for forests from coastal Gabon, in large
224 areas from DRC and in the northern margin of the forest domain. Forests from
225 Cameroon and in the south of the Republic of Congo mostly appear vulnerable due to
226 the high expected human impact on forests by 2085 (orange patches in Fig. 4A). By
227 contrast, the tri-national Sangha transboundary forest complex and the northeastern
228 part of Gabon appeared as the least vulnerable area in the region (the large green
229 patch in Fig. 4A). Globally, DRC, which comprises most of the central African forests,
230 mainly contains forests that are predicted to be vulnerable to climate change and/or to
231 anthropogenic pressure (blues to pink patches in Fig. 4A).

232 **Conclusions and perspectives**

233 While some country-specific vegetation patterns were already suggested by
234 phytogeographers, here we provide the first synoptic view of central African forest
235 composition at a fine resolution, based on an unprecedented amount of quantitative
236 data. Unveiling the functional composition of central African forests conveys important
237 insights on their functioning, dynamics and carbon uptake potential and on the way they
238 could respond to global change. Accounting for forest functional characteristics can also
239 considerably reduce uncertainty in large-scale vegetation models⁴⁴ or improve remote

240 sensing approaches, for example, by assimilating large-scale variation in wood density
241 into forest carbon maps⁴⁵. Our maps may also help scientists to design representative
242 sampling to better understand the long-term impact of climate change on tree species
243 and stand dynamics, e.g., monitoring under-represented forest types or areas highly
244 vulnerable to climate change.

245 The forest types and vulnerability maps should guide the development of new land use
246 plans that preserve the full range of evolutionary and functional potential of today's
247 forests or, at least, that maintain their connectivity to attenuate the threats related to
248 expected changes. In central Africa, protected areas and logging concessions, which
249 cover almost half of the forest domain (14.9% and 32.2%, respectively; Extended Data
250 Fig. 9), are important to consider in such plans. Protected areas do not equally cover
251 the ten identified forest types (4 to 54%; Extended Data Table 1) and should therefore
252 be extended to reach a better representativity. How estimated vulnerability should be
253 accounted for when designing protected areas, e.g., by extending the network in
254 vulnerable areas to minimize biodiversity loss, or in areas with low anthropogenic
255 pressure to improve their protection, is subject to debate⁴⁶. Logging concessions can
256 also contribute to the maintenance of forest cover and functions, providing that they are
257 well managed^{47,48}, and currently likely act like biodiversity corridors between protected
258 areas⁴⁹. However, this will only prove effective in the long term if they strictly comply
259 with legislation and, ideally, with standard certification requirements. These good
260 practices are especially important in forests dominated by evergreen taxa with high
261 wood density, where disturbances may have a higher impact on community
262 composition. In areas expected to be under high anthropogenic pressure, forest
263 connectivity could be preserved by promoting agroforestry and restoration programs,
264 strictly controlling access to logging roads and stabilizing shifting agriculture⁵⁰. Over
265 central Africa, the highest uncertainties for the future of forests remain in DRC, where
266 substantial areas, belonging to the state, are not yet attributed to any land use category
267 and should deserve particular attention due to their high vulnerability (Fig. 4).

268

269 **Main references**

- 270 1. Diffenbaugh, N. S. & Giorgi, F. Climate change hotspots in the CMIP5 global climate
271 model ensemble. *Climatic change* **114**, 813–822 (2012).
- 272 2. United Nations, Department of Economic and Social Affairs, Population Division.
273 World Population Prospects: The 2017 Revision, Key Findings and Advance Tables.
274 *Working Paper ESA/P/WP/248*, (2017).
- 275 3. Malhi, Y., Adu-Bredu, S., Asare, R. A., Lewis, S. L. & Mayaux, P. African rainforests:
276 Past, present and future. *Philosophical Transactions of the Royal Society B: Biological*
277 *Sciences* **368**, 20120312 (2013).
- 278 4. James, R., Washington, R. & Rowell, D. P. Implications of global warming for the
279 climate of African rainforests. *Philosophical Transactions of the Royal Society B:*
280 *Biological Sciences* **368**, 20120298 (2013).
- 281 5. Abernethy, K., Maisels, F. & White, L. J. Environmental issues in central Africa.
282 *Annual Review of Environment and Resources* **41**, 1–33 (2016).
- 283 6. Hubau, W. *et al.* Asynchronous carbon sink saturation in African and Amazonian
284 tropical forests. *Nature* **579**, 80–87 (2020).
- 285 7. De Wasseige, C., Tadoum, M., Atyi, E. & Doumenge, C. *The forests of the Congo*
286 *Basin-Forests and climate change*. (Weyrich, 2015).
- 287 8. Stévant, T. *et al.* A third of the tropical African flora is potentially threatened with
288 extinction. *Science advances* **5**, eaax9444 (2019).
- 289 9. Parmentier, I. *et al.* The odd man out? Might climate explain the lower tree alpha-
290 diversity of African rain forests relative to Amazonian rain forests? *Journal of Ecology*
291 **95**, 1058–1071 (2007).

- 292 10. Réjou-Méchain, M. *et al.* Regional variation in tropical forest tree species
293 composition in the Central African Republic: An assessment based on inventories by
294 forest companies. *Journal of Tropical Ecology* **24**, 663–674 (2008).
- 295 11. Réjou-Méchain, M. *et al.* Tropical tree assembly depends on the interactions
296 between successional and soil filtering processes. *Global Ecology and Biogeography*
297 **23**, 1440–1449 (2014).
- 298 12. Fayolle, A. *et al.* Geological substrates shape tree species and trait distributions in
299 african moist forests. *PLoS ONE* **7**, e42381 (2012).
- 300 13. Fayolle, A. *et al.* Patterns of tree species composition across tropical African forests.
301 *Journal of Biogeography* **41**, 2320–2331 (2014).
- 302 14. Droissart, V. *et al.* Beyond trees: Biogeographical regionalization of tropical Africa.
303 *Journal of biogeography* **45**, 1153–1167 (2018).
- 304 15. Sosef, M. S. *et al.* Exploring the floristic diversity of tropical Africa. *BMC biology* **15**,
305 15 (2017).
- 306 16. Parmentier, I. *et al.* Predicting alpha diversity of African rain forests: Models based
307 on climate and satellite-derived data do not perform better than a purely spatial model.
308 *Journal of Biogeography* **38**, 1164–1176 (2011).
- 309 17. Bry, X., Trottier, C., Verron, T. & Mortier, F. Supervised component generalized
310 linear regression using a pls-extension of the fisher scoring algorithm. *Journal of*
311 *Multivariate Analysis* **119**, 47–60 (2013).
- 312 18. Steege, H. ter *et al.* Continental-scale patterns of canopy tree composition and
313 function across Amazonia. *Nature* **443**, 444–447 (2006).
- 314 19. Slik, J. F. *et al.* Soils on exposed Sunda Shelf shaped biogeographic patterns in the
315 equatorial forests of Southeast Asia. *Proceedings of the National Academy of Sciences*
316 **108**, 12343–12347 (2011).

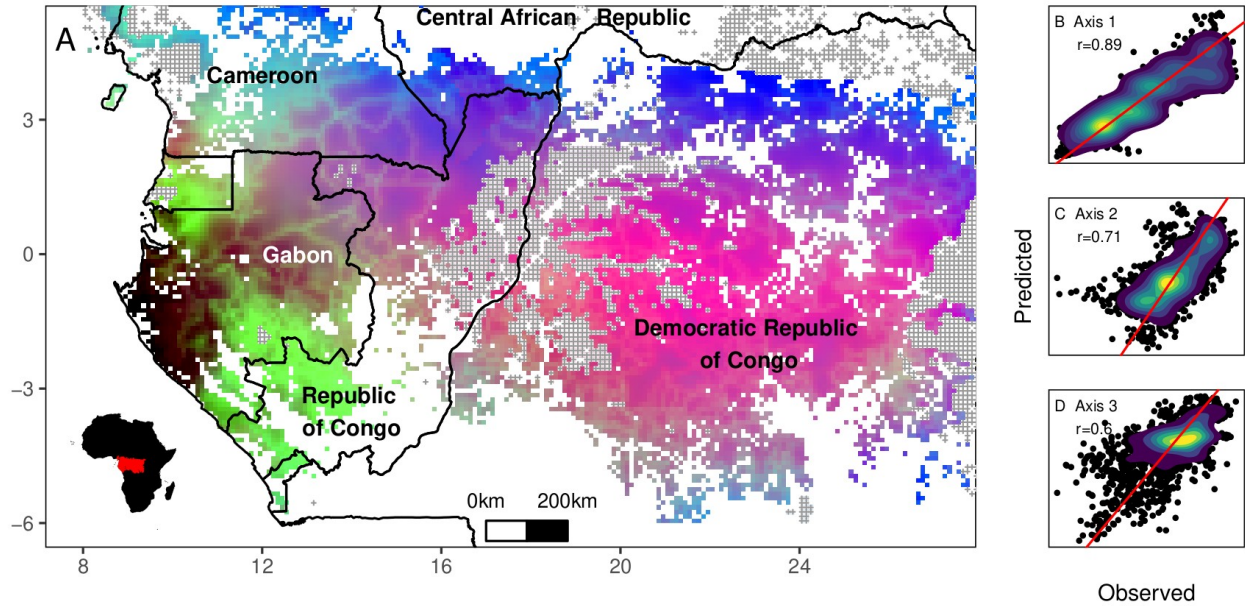
- 317 20. Philippon, N. *et al.* The light-deficient climates of western Central African evergreen
318 forests. *Environmental Research Letters* **14**, 034007 (2019).
- 319 21. Sullivan, M. J. P. *et al.* Long-term thermal sensitivity of Earth's tropical forests.
320 *Science* **368**, 869–874 (2020).
- 321 22. Beale, C. M., Lennon, J. J. & Gimona, A. Opening the climate envelope reveals no
322 macroscale associations with climate in European birds. *Proceedings of the National*
323 *Academy of Sciences* **105**, 14908–14912 (2008).
- 324 23. Deblauwe, V. *et al.* Remotely sensed temperature and precipitation data improve
325 species distribution modelling in the tropics. *Global Ecology and Biogeography* **25**, 443–
326 454 (2016).
- 327 24. Maguire, K. C. *et al.* Controlled comparison of species-and community-level models
328 across novel climates and communities. *Proc. R. Soc. B* **283**, 20152817 (2016).
- 329 25. Morin-Rivat, J. *et al.* Present-day central African forest is a legacy of the 19th
330 century human history. *Elife* **6**, (2017).
- 331 26. Ricklefs, R. E. Intrinsic dynamics of the regional community. *Ecology Letters* **18**,
332 497–503 (2015).
- 333 27. Violle, C. *et al.* Let the concept of trait be functional! *Oikos* **116**, 882–892 (2007).
- 334 28. Díaz, S. *et al.* The global spectrum of plant form and function. *Nature* **529**, 167–171
335 (2016).
- 336 29. Rüger, N. *et al.* Demographic trade-offs predict tropical forest dynamics. *Science*
337 **368**, 165–168 (2020).
- 338 30. Ouédraogo, D.-Y. *et al.* The determinants of tropical forest deciduousness:
339 Disentangling the effects of rainfall and geology in central Africa. *Journal of Ecology*
340 **104**, 924–935 (2016).

- 341 31. Shipley, B. *From plant traits to vegetation structure: Chance and selection in the*
342 *assembly of ecological communities*. (Cambridge University Press, 2010).
- 343 32. Feeley, K. J. & Silman, M. R. Biotic attrition from tropical forests correcting for
344 truncated temperature niches. *Global Change Biology* **16**, 1830–1836 (2010).
- 345 33. Parry, M. *et al.* *Climate change 2007-impacts, adaptation and vulnerability: Working*
346 *group II contribution to the fourth assessment report of the IPCC*. **4**, (Cambridge
347 University Press, 2007).
- 348 34. Foden, W. B. *et al.* Identifying the world's most climate change vulnerable species:
349 A systematic trait-based assessment of all birds, amphibians and corals. *PloS one* **8**,
350 (2013).
- 351 35. Lachenaud, O., Stévant, T., Ikabanga, D., Ndjabounda, E. C. N. & Walters, G. The
352 littoral forests of the Libreville area (Gabon) and their importance for conservation:
353 Description of a new endemic species (Rubiaceae). (2013).
354 doi:[info:doi/10.5091/plecevo.2013.744](https://doi.org/10.5091/plecevo.2013.744)
- 355 36. Aguirre-Gutiérrez, J. *et al.* Drier tropical forests are susceptible to functional
356 changes in response to a long-term drought. *Ecology Letters* **22**, 855–865 (2019).
- 357 37. Claeys, F. *et al.* Climate change would lead to a sharp acceleration of Central
358 African forests dynamics by the end of the century. *Environmental Research Letters* **14**,
359 044002 (2019).
- 360 38. McDowell, N. G. *et al.* Pervasive shifts in forest dynamics in a changing world.
361 *Science* **368**, (2020).
- 362 39. Zhou, L. *et al.* Widespread decline of Congo rainforest greenness in the past
363 decade. *Nature* **509**, 86 (2014).
- 364 40. Purvis, A. Phylogenetic Approaches to the Study of Extinction. *Annual Review of*
365 *Ecology, Evolution, and Systematics* **39**, 301–319 (2008).

- 366 41. Yachi, S. & Loreau, M. Biodiversity and ecosystem productivity in a fluctuating
367 environment: The insurance hypothesis. *Proceedings of the National Academy of*
368 *Sciences* **96**, 1463–1468 (1999).
- 369 42. Neves, D. M. *et al.* Evolutionary diversity in tropical tree communities peaks at
370 intermediate precipitation. *Scientific reports* **10**, 1–7 (2020).
- 371 43. Letcher, S. G. Phylogenetic structure of angiosperm communities during tropical
372 forest succession. *Proceedings of the Royal Society B: Biological Sciences* **277**, 97–104
373 (2010).
- 374 44. Fyllas, N. M., Quesada, C. A. & Lloyd, J. Deriving Plant Functional Types for
375 Amazonian forests for use in vegetation dynamics models. *Perspectives in Plant*
376 *Ecology, Evolution and Systematics* **14**, 97–110 (2012).
- 377 45. Mitchard, E. T. A. *et al.* Markedly divergent estimates of Amazon forest carbon
378 density from ground plots and satellites. *Global Ecology and Biogeography* **23**, 935–946
379 (2014).
- 380 46. Visconti, P., Pressey, R. L., Bode, M. & Segan, D. B. Habitat vulnerability in
381 conservation planning—when it matters and how much. *Conservation Letters* **3**, 404–
382 414 (2010).
- 383 47. Putz, F. E. *et al.* Sustaining conservation values in selectively logged tropical
384 forests: The attained and the attainable. *Conservation Letters* **5**, 296–303 (2012).
- 385 48. Gourlet-Fleury, S. *et al.* Tropical forest recovery from logging: A 24 year silvicultural
386 experiment from Central Africa. *Phil. Trans. R. Soc. B* **368**, 20120302 (2013).
- 387 49. Clark, C. J., Poulsen, J. R., Malonga, R. & Jr, P. W. E. Logging Concessions Can
388 Extend the Conservation Estate for Central African Tropical Forests. *Conservation*
389 *Biology* **23**, 1281–1293 (2009).
- 390 50. Curtis, P. G., Slay, C. M., Harris, N. L., Tyukavina, A. & Hansen, M. C. Classifying
391 drivers of global forest loss. *Science* **361**, 1108–1111 (2018).

392

393 **Figures**

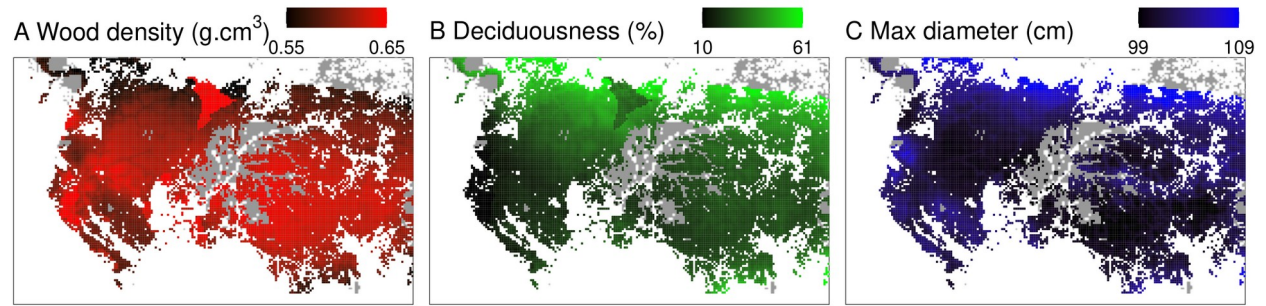


394

395 **Figure 1: Floristic composition of central African forests.** **A**, Spatialized RGB
396 composition of the three first axes of a correspondence analysis (CA) performed on
397 jointly predicted taxon abundances at 10-km resolution ($n=193$ taxa; axis 1: blue, axis 2:
398 red, axis 3: green). Grey crosses represent forested areas outside the calibration
399 domain, including permanently flooded forests and country boundaries are represented
400 in black. Right panels **B-D** provide cross-validation results comparing the observed and
401 predicted CA gradients (1:1 line in red). Taxon CA planes 1-2 and 1-3 are given in
402 Extended Data Fig. 2.

403

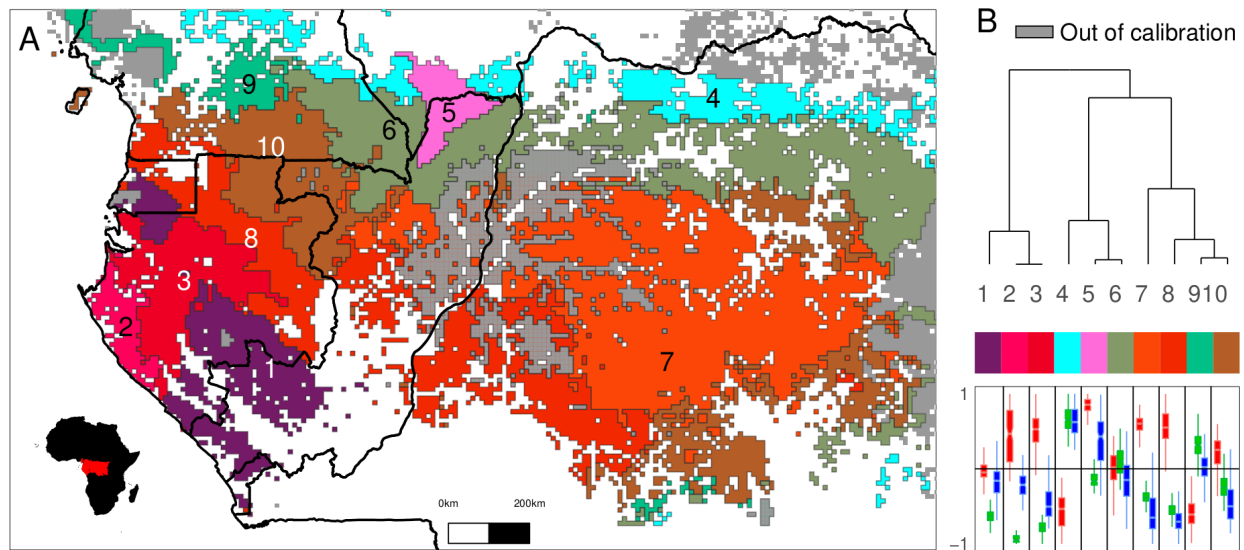
404



405

406 **Figure 2: Predicted functional composition of central African forests. A-C,**

407 Predicted community weighted functional trait values at 10-km resolution.



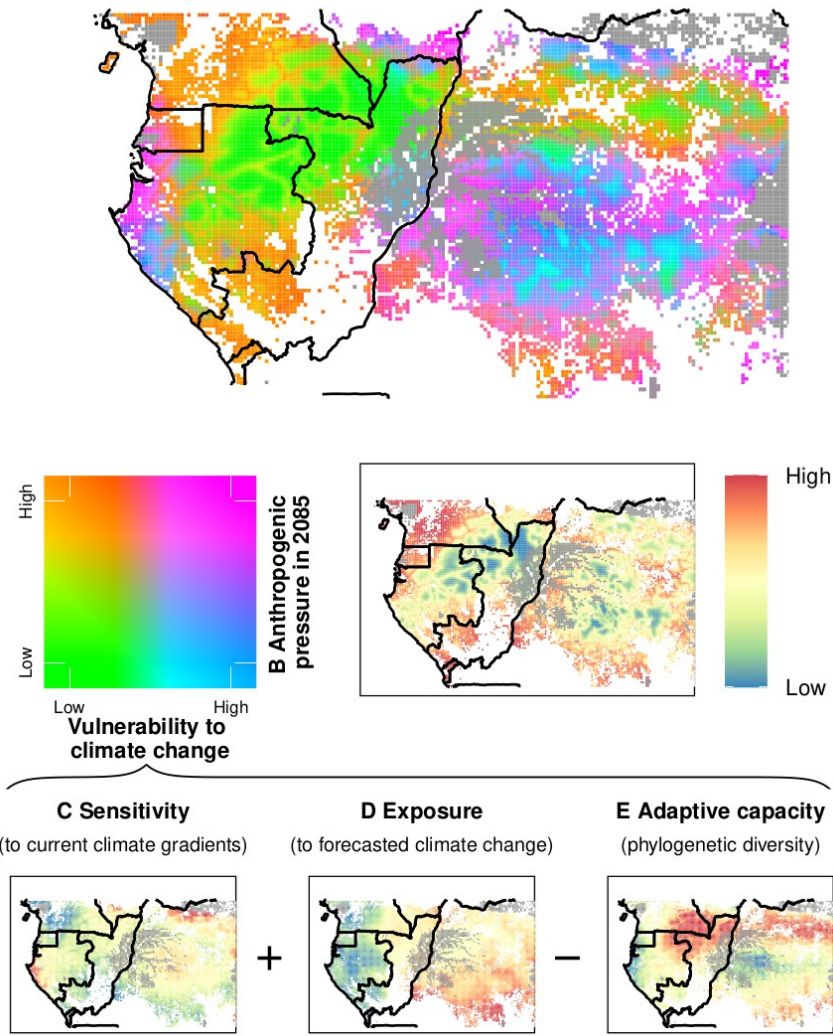
408

409 **Figure 3: Main forest types across central Africa and their functional composition.**

410 **A**, Forest type classification obtained by hierarchical clustering of the predicted floristic
 411 gradients. Colors represent a RGB composite of the mean values of the three functional
 412 traits per forest type (see Fig. 2), viz. wood density (red), deciduousness (green) and
 413 maximum diameter (blue). Thus similar colors illustrate similar functional composition.

414 **B**, Taxonomic relationships among the forest types illustrated by a clustering
 415 dendrogram (top) and a boxplot of the standardized predicted functional composition
 416 over the 12,295 grid cells (bottom), with wood density in red, deciduousness in green
 417 and maximum diameter in blue (median is reported at the center, the lower and upper
 418 hinges correspond to the first and third quartiles and the two whiskers extend from
 419 these two quartiles to the largest and smallest values, at most 1.5 times the inter-
 420 quartile range from the hinge). Forest type names and additional information are
 421 provided in Extended Data Table 1. Clustering uncertainty is reported in Fig. S1.

A Vulnerability to global change



422

423 **Figure 4: Predicted vulnerability of central African tree communities to global**
424 **changes. A,** Composite map of the vulnerability to climate change and of the
425 forecasted human-induced forest disturbance intensity by 2085. **B,** Projected human-
426 induced forest disturbance intensity in 2085. Vulnerability to climate change was
427 estimated as the sensitivity to current climate (**C**) plus the exposure to forecasted
428 climate changes by 2085 (under RCP scenario 4.5) (**D**) minus the adaptive capacity of
429 tree communities using phylogenetic diversity as a proxy (**E**).

430

431 **METHODS**

432 **Floristic and functional trait data**

433 Forestry data were extracted from management forest inventories conducted in 105
434 logging concessions covering ca. 1.6×10^5 km² (Extended Data Fig. 1). Most companies
435 followed a standardized inventory protocol similar to that described in Réjou-Méchain et
436 al.⁵¹. In most cases, it consisted of continuous and parallel transects 20 m or 25 m wide,
437 often 2-3 km apart, and subdivided into rectangular 0.4 or 0.5-ha plots. Overall, the full
438 dataset had a total of 192,972 plots. Within each plot, trees with a diameter at breast
439 height (DBH) ≥ 30 cm were allocated into 10-cm wide diameter classes and identified at
440 the species or genus level whenever possible through either commercial or local
441 names⁵¹. Independent analyses performed on 298 scientific plots (≥ 1 ha in size)
442 showed that the floristic gradients obtained with large trees are representative of the
443 ones obtained with trees ≥ 10 cm in diameter (Pearson $r > 0.94$; Fig. S4). Overall, ca.
444 7×10^6 trees were recorded. Taxonomy was revised and homogenized using the African
445 Flowering Plants Database ([http://www.ville-ge.ch/musinfo/bd/cjb/africa/index.php?](http://www.ville-ge.ch/musinfo/bd/cjb/africa/index.php?langue=an)
446 [langue=an](http://www.ville-ge.ch/musinfo/bd/cjb/africa/index.php?langue=an), last access on 01/09/2019) and the Angiosperm Phylogeny Group III for
447 orders and families⁵². A total of 1,092 taxa were recorded in the original dataset.
448 Extensive botanical controls demonstrated that the patterns of both intra (alpha)- and
449 inter (beta)- plot diversity extracted from these data were highly reliable⁵¹.
450 For the purpose of the present paper, we conducted an additional assessment
451 according to botanical experts and by comparing the distributional range of our taxa with
452 that in other datasets^{53,54} to select a set of species and genera deemed to be reliably
453 identified over the whole study area ($n=195$). The abundances of these taxa were
454 aggregated in 10x10-km² grid cells across the study area, but we only kept the taxa
455 occurring in at least 5% of the cells to discard taxa that cannot be studied at the regional
456 scale ($n=2$). For the statistical analyses, we kept the 10x10-km² grid cells having a field
457 plot sampling area \geq to 10 ha and where the selected taxa represented at least 75% of
458 the total number of individuals originally inventoried to ensure that our dataset was
459 representative of the within-cell tree community composition. The final dataset contains

460 6.1×10^6 tree individuals belonging to 193 taxa, of which 96 were analyzed at the
461 species and 97 at the genus levels (Table S2), recorded in 185,665 plots aggregated in
462 1,571 10x10-km² grid cells. Overall, the selected taxa represented 90% of the total
463 number of individuals originally inventoried in the selected grid cells.

464 For each taxon, we compiled information on three important functional traits. First, we
465 extracted an average wood density using the global wood density database^{55,56} as well
466 as other wood density data⁵⁷. Wood density is an integrative trait that reflects a trade-off
467 between tree growth potential and mortality risk²⁸ and is thus highly informative on
468 community dynamics⁵⁸. It ultimately directly impacts the amount of carbon that can be
469 stored in the vegetation⁵⁹. Second, we extracted the leaf phenology (deciduous or
470 evergreen) of all taxa from the large unpublished CoForTraits database⁶⁰. This database
471 compiles information on more than 1000 species from central Africa with values
472 extracted from the literature (mostly from local floras, academic papers and unpublished
473 theses). When several values were available for a given species from different sources,
474 we attributed the one with the maximum of occurrences (ambiguities were left as
475 unknown). At the genus level, we first computed this step for all species belonging to
476 the genus and then attributed the phenology with the maximum of occurrences at the
477 species level to the genus so that all congeneric species have the same weight in the
478 phenology attribution. This approach relies on the assumption that leaf phenological
479 traits are highly phylogenetically conserved⁶¹. For a few taxa (n=5), the phenology
480 information was obtained from Ouédraogo et al.³⁰ and following these authors we
481 considered *Lophira alata* Banks ex C. F. Gaertn. and *Musanga cecropioides* R. Br. as
482 leaf exchangers, i.e., with a trait value of 0.5, intermediate between evergreen (0) and
483 deciduous (1). Leaf phenology is one of the few traits considered in dynamic global
484 vegetation models as it impacts the dynamics of forest productivity⁶². In particular,
485 deciduousness indicates that tree photosynthetic activity, and thus growth, is seasonally
486 depressed, which has a direct impact on carbon, water and nutrient cycling⁶³.
487 Deciduousness has often been interpreted as a strategy to avoid water stress and is
488 thus expected to depend on climate and soil conditions^{30,64}. Lastly, we used the original

489 inventory data to calculate the maximum diameter as the 95th percentile value of the
490 diameter distribution for each taxon. Maximum potential diameter, which is often used
491 as a proxy of maximum height⁶⁵, informs both on tree competitive ability for light and on
492 the carbon sequestration potential. At the community level, it is expected to vary along
493 gradients of productivity and disturbance⁶⁶. Leaf phenology was successfully assigned
494 to 89% of the taxa (98% of the individuals), wood density to 91% of the taxa (96% of the
495 individuals) and maximum diameter to all taxa.

496 **Climate and soil data**

497 We considered 24 climatic predictors derived from the open Climatic Research Unit
498 (CRU) dataset⁶⁷ (Extended Data Table 2). We decided to rely on the CRU dataset as
499 other datasets, such as WorldClim⁶⁸, contain erroneous observations for some climatic
500 stations (e.g., Ngoundi in Cameroon) that severely impacted our model. Furthermore,
501 our cross-validation approach showed that the CRU database led to higher correlations
502 between observed and predicted taxa abundances, correspondence analyses scores
503 and community weighted trait values than the WorldClim⁶⁸ and CHIRPS⁶⁹ databases
504 (results not shown).

505 Soil maps have been published at the country scale in central Africa and their
506 homogenization is very challenging. We thus relied on a global dataset, the Harmonized
507 World Soil Database (HWSD)⁷⁰, to attribute a soil type to each grid cell. A cross-
508 validation analysis of our joint distribution model revealed that soil significantly improved
509 predictions, mostly due to the contrast between Arenic Acrisols and the other soil types
510 (Fig. S5). To keep the model parsimonious and maximize its robustness, we thus
511 merged all soil categories but the Arenic Acrisols soils into a single category and
512 discarded the permanently flooded areas as mapped in the open ESA-CCI landcover
513 product (V.1.6), where no tree inventory data were available.

514 **Human-induced forests disturbance intensity**

515 Many studies have attempted to spatialize human impacts on environment at a large
516 scale. In most cases, these human footprint maps have consisted of cumulative threat

517 maps, assuming for instance population density and infrastructure effects^{71–73}.
518 Moreover, most of these maps relied on population statistics obtained at the level of
519 administrative entities, resulting in human footprint indices with sharp changes at
520 administrative boundaries⁷⁴. We thus developed a statistical model to link the probability
521 for a forest pixel i to be impacted by anthropogenic activities depending on human
522 population density and road proximity through nonlinear relationships. This resulted in a
523 spatially continuous index representing human-induced forest disturbance intensity that
524 can be projected in space and/or time following predefined human population dynamics
525 scenarios (Extended Data Fig. 8).

526 We calibrated this index with the “Settlement Points” dataset produced under the
527 “Global Rural Urban Mapping Project” ([Grumpv1](#)). This dataset provides estimates of
528 human population (counts, in persons) for the year 2000 using a proportional allocation
529 gridding algorithm (1-km² grid) based on more than 1,000,000 national and subnational
530 geographic units. Focusing on central Africa, we compared this product with the Natural
531 Earth Populated Places product (version 3.0.0;
532 [http://www.naturalearthdata.com/downloads/10m-cultural-vectors/10m-populated-](http://www.naturalearthdata.com/downloads/10m-cultural-vectors/10m-populated-places/)
533 [places/](http://www.naturalearthdata.com/downloads/10m-cultural-vectors/10m-populated-places/); last access the 07/10/2018) derived from the LandScan
534 ([https://earthworks.stanford.edu/catalog/stanford-yj715rc4110#iso-metadata-reference-](https://earthworks.stanford.edu/catalog/stanford-yj715rc4110#iso-metadata-reference-info)
535 [info](https://earthworks.stanford.edu/catalog/stanford-yj715rc4110#iso-metadata-reference-info)) dataset (pixels with fewer than 200 persons per km² were discarded). The total
536 number of populated points in central Africa (longitude 5.6 to 39.8, latitude -9.8 to 7.5 in
537 decimal degrees) was 807 and 376 for the Grumpv1 and Natural Earth products,
538 respectively. We thus performed a random manual check of the populated places
539 present in Grumpv1 and absent from Natural Earth (the reverse rarely occurred) using
540 Google Earth images and found that in all cases Grumpv1 was correct. We thus finally
541 used the Grumpv1 dataset, which mostly provides information on populated places with
542 more than ca. 1000 people. Because smaller populations may have a significant impact
543 on forests, we added to this dataset the populated locations of the category “towns”
544 from OpenStreetMap (<https://data.maptiler.com/downloads/planet/#1.59/-17.3/19.7>; last
545 access 02/10/2018) assuming by default that they all contained 500 people
546 (OpenStreetMap does not provide systematic information on population size).

547 The road network was extracted from the Global Roads Open Access Data Set, version
 548 1 (<https://data.maptiler.com/downloads/planet/#1.59/-17.3/19.7>; last access the
 549 14/09/2018) a dataset combining road data by country. Note that logging roads are not
 550 fully represented in this dataset, so we may underestimate their effect in this study. A
 551 few roads from the northern Republic of Congo were corrected using data from
 552 OpenStreetMap. Preliminary analyses revealed that further accounting for the railway
 553 and river networks did not improve predictions of tree taxon and community
 554 distributions.

555 Our index was thus calculated as followed. Let $z_i, i=1, \dots, n$ be n random variables
 556 indicating the disturbance status of pixel i : 0 if the pixel is undisturbed and 1 if disturbed.

557 We assumed that z_i is distributed as a Bernoulli variable: $z_i = \text{Bern}(p_i)$ with $p_i = \frac{IP_i(\theta)}{IP_i(\theta) + IR_i^r}$

558 where $IP_i(\theta)$ is a synthetic index describing the influence of the population density of all
 559 populated places on pixel i (see below), θ is an unknown parameter to be inferred, and
 560 IR_i^r expresses the road influence on pixel i , defined as the normalized square root
 561 distance of pixel i to the nearest road r :

$$562 \quad IR_i^r = \frac{\min_{r \in R} \sqrt{DR_i^r}}{\max_{i=1, \dots, n} \left(\min_{r \in R} \sqrt{DR_i^r} \right)}$$

563
 564 where DR denotes the distance to the nearest road in the study area and R denotes all
 565 roads in the study area.

566 Population influence, IP_i^θ , is defined as the normalized square root of the weighted sum
 567 of the population size of place j . Note that the weight depends on both the distance
 568 between pixel i and populated place j , δ_{ij} , and on the population size N_j :

$$IP_i^\theta = \frac{\sqrt{\sum_j^n N_j e^{-\frac{\delta_{ij}}{\log(N_j)^\theta} + 1}}}{\max \sqrt{\sum_j^n N_j e^{-\frac{\delta_{ij}}{\log(N_j)^\theta} + 1}}}$$

570 We finally calibrated the θ parameter using two reference areas of ca. 190,000 km² (Fig.
 571 S6). These two areas were chosen because they cover contrasting conditions, are well
 572 known by our team and were found to be little influenced by atmospheric pollution in the
 573 MODIS data. Degraded versus intact forests were identified from a recently published
 574 MODIS-based regional vegetation map²⁰. Using a likelihood optimization approach in
 575 these two areas, we obtained $\theta=1.27$ and 1.71 in calibration areas 1 and 2, respectively,
 576 indicating that under a similar anthropogenic context, forests tend to be disturbed at a
 577 greater distance from anthropogenic disturbance sources in the second calibration area.
 578 The final human-induced forest disturbance intensity index was thus calculated with θ
 579 $=1.49$, the average estimate for the two calibration areas, over the whole central African
 580 forest domain, thus avoiding the risk of artefacts related to atmospheric pollution from
 581 which suffer satellite products, especially over Gabon.

582 This index, built independently from our floristic dataset, outperformed previously
 583 published indices to predict floristic composition in our study area. Using a simple linear
 584 model, with individual anthropogenic indices as single predictors, the mean wood
 585 density of tree communities was better predicted with our new index ($r=0.33$) than with
 586 the WorldPop⁷⁵ ($r=0.30$), LandScan ($r=0.15$) and Venter⁷² ($r=0.23$) indices. Similarly,
 587 using a simple generalized linear model with a Poisson distribution to predict the
 588 abundance of *Musanga cecropioides*, the most widespread and abundant short-lived
 589 pioneer taxon over central African forests, revealed a better performance of our index
 590 ($r=0.35$) compared to previous indices ($r=0.31, 0.11, 0.26$ for WorldPop, LandScan and
 591 Venter, respectively).

592 **Statistical model**

593 To predict the joint taxa distributions we relied on a recently developed methodology
594 called supervised component generalized linear regression (SCGLR)¹⁷, which identifies
595 the most predictive dimensions among a large set of potentially multicollinear predictors.
596 SCGLR is an extension of partial least-squares regression (PLSR) to the uni- and
597 multivariate generalized linear framework. PLSR is particularly well suited for analyzing
598 a large array of correlated predictor variables, and many studies have demonstrated its
599 ability for prediction in various biological fields, such as genetics⁷⁶ or ecology⁷⁷. While
600 PLSR is well adapted for continuous variables, SCGLR is suited for non-Gaussian
601 outcomes and noncontinuous covariates. It is a model-based approach that extends
602 PLSR⁷⁸, PCA on instrumental variables⁷⁹, canonical correspondence analysis⁸⁰, and
603 other related empirical methods by maximizing a trade-off between goodness of fit of
604 the model and the quantity of information the components capture from the climatic
605 variables. This information is measured through an indicator of “structural relevance”
606 (SR)⁸¹, which uses bundles of highly correlated variables to attract components to rich
607 and robust informational dimensions.

608 The components are sought as K linear combinations of environmental variables
609 common to all species with coefficient vectors denoted $u=(u_1, \dots, u_K)$ (under norm and
610 orthogonality constraints). SCGLR also estimates the corresponding $q \times K$ (number of
611 species by number of components) matrix of unknown parameters γ to maximize the
612 following convex sum:

$$613 \quad s \log \psi(u, \gamma) + (1-s) \log \phi_l(u)$$

614 where ψ is the likelihood and ϕ_l is the SR. s and l are tuning parameters. s is related to
615 the trade-off between goodness of fit and structural relevance. l is a nonnegative scalar
616 related to the narrowness of the bundles of climatic variables the components are
617 wanted to align with. The K climatic components (CCs) are then equal to
618 $CC_k = Xu_k, k=1, \dots, K$ and can be understood as the main environmental directions
619 predicting all species simultaneously, while $\gamma_j, j=1, \dots, q$ are the magnitude of the effects
620 of the K components on the abundances of each species. Then, the species

621 abundances of each taxon $j=1, \dots, 193$ on the grid cell $i=1, \dots, 1571$ are modeled using a
622 generalized linear Poisson regression such that:

$$623 \quad y_{ij} \sim P(S_i \lambda_{ij})$$

$$624 \quad \log(\lambda_{ij}) = X_i \beta_j + T_i \alpha_j = X_i u \gamma_j + T_i \alpha_j = C C_i \gamma_j + T_i \alpha_j$$

625 where X denotes climatic variables (Extended data Table 2), S_i is an offset
626 corresponding to the number of plots within each grid cell, and T is a set of covariates
627 known to impact species abundances: here, the soil type and the human-induced forest
628 disturbance intensity index, as well as its logarithm to account for nonlinear responses.
629 The number of components (K) as well as the tuning parameters (l and s) must
630 appropriately be chosen. This was done with a 10% cross-validation procedure in which
631 the criterion used was the harmonic mean of the mean square prediction error (MSPE)
632 across the 194 taxa. A dedicated R package, SCGLR⁸², is available (see also
633 <https://github.com/SCnext/SCGLR>).

634 To assess the predictive power of our model, we performed a leave-one block out
635 cross-validation in which our dataset was divided into 40 spatial clusters identified with a
636 Ward's hierarchical clustering⁸³ of plot coordinates (Fig. S7). All clusters but one were
637 used for training the model (i.e., calibration dataset) and the remaining cluster was used
638 for validating the model. We repeated this procedure 40 times such that all clusters
639 were used once in the validation dataset and participated in the model assessment.
640 Model validation was performed through the use of the nonparametric Spearman's rank
641 correlation coefficients between observations and predictions. For individual taxon
642 abundances, correlations were estimated using observed and predicted abundance per
643 taxon. For taxon assemblages, a correspondence analysis (CA) was performed on the
644 grid cell \times observed species abundance matrix, providing the observed CA axes. The
645 predicted site scores on each CA axis were then obtained by projecting the grid cell \times
646 predicted species abundance matrix in the observed CA planes. Correlations were
647 computed on the observed and predicted site scores (i.e., loadings) enabling us to
648 assess the ability of our model to predict the main floristic gradients across our area.

649 Finally, for the three functional traits, correlations were estimated on the grid cell-based
650 community weighted mean (CWM) traits²⁷ calculated on observed and predicted taxon
651 assemblages.

652 Taxon abundances and community composition were predicted across the entire study
653 area in a regular 10-km grid. To predict the floristic composition of the existing forests,
654 we first used the ESA-CCI landcover product (V.1.6) to only keep grid cells that are
655 likely to be forested (i.e., category “broadleaved evergreen”). Then, we only selected
656 grid cells that had a combination of predictor values similar to those in the calibration
657 dataset. To do this, we used a 3-dimensional convex hull algorithm on the three climatic
658 components to exclude all the grid cells that had a combination of predictors different
659 from that represented in the calibration dataset. This resulted in 12,295 grid cells,
660 representing 85% of the central African forests, i.e., an area of ca. 1,230,000 km².
661 We finally used the Ward’s hierarchical clustering method to classify the predicted
662 floristic composition into broad floristic types. Group classification was done on the first
663 five axes of a CA performed on predicted taxon abundances, accounting for 77% of the
664 total inertia. The number of retained types was chosen based on our expert knowledge.
665 The uncertainty associated with this classification was then assessed through Gaussian
666 finite mixture models⁸⁴ (repeated 500 times) using a spherical, equal volume model
667 (EII).

668 **Spatially explicit null models**

669 Whenever predictors and observations are spatially structured, model errors of type I
670 (false positive associations) are inflated⁸⁵, hindering our capacity to extrapolate
671 predictions in space or time²². We thus built a spatialized null model to test the degree
672 to which the successfulness of our predictions resulted from an actual relationship with
673 climatic variables or was simply due to spatial costructures between taxon distributions
674 and climatic gradients that arose by chance. We used the RGEOSTAT R package⁸⁶ to
675 simulate sets of SCGLR climatic components (CCs) having similar spatial properties to
676 those of the observed CCs as well as similar spatial costructures between them. This
677 step consisted of fitting theoretical variograms and covariograms to empirical ones to

678 simulate random realizations that can be then used as “null” spatialized predictors (Fig.
679 S8 and S9). We simulated 500 sets of “null” spatialized predictors and used them as
680 predictors in our GLMs using the leave-one block out cross-validation described above.
681 The resulting correlations between observed and predicted taxon abundances, and
682 axes scores (for taxon assemblages) were finally compared with the correlations
683 obtained when observed climatic predictors were considered. The resulting p-values
684 were calculated as the number of times a simulated correlation was higher than the
685 observed one, divided by the total number of realizations (n=501).

686 **Forest vulnerability to global change**

687 Vulnerability to climate change, as assessed through the IPCC framework, is composed
688 of three components: (1) sensitivity, (2) exposure, and (3) adaptive capacity to climate
689 change.

690 Sensitivity to climate change, $Sensitivity_{clim}$, was firstly estimated at the taxon level in
691 a similar way to Foden et al.³⁴. For each taxon, we calculated the mean of the weighted
692 standard deviation (SD_w) of the three climatic components (CCs) at the present time,
693 using locally observed taxon abundances as weights. SD_w thus represents the width of
694 the climatic niche currently occupied by the taxa. Taxon-specific climate sensitivity was
695 then measured as $1/SD_w$ (it increases as niche width decreases). To upscale tree
696 sensitivity to climate change at the community level and over our study area, sensitivity
697 was measured as the community weighted mean (CWM) of taxon-specific climate
698 sensitivity scores, using predicted taxon assemblages.

699 Exposure to climate change, $Exposure_{clim}$, was assessed using projected changes in
700 climate from 18 unique climate model combinations provided by the AFRICLIM V3.0
701 dataset⁸⁷ (last access on 03/02/2020). These models corresponded to pairwise
702 combinations of five regional climate models (RCMs) driven by ten general circulation
703 models (GCMs), with an unequal number of GCMs models per RCM (ten models for the
704 Swedish Meteorological and Hydrological (SMHI) RCM, four for the Climate Limited-
705 area Modelling Community (CLMCOM) RCM, two for the Royal Netherlands

706 Meteorological Institute (KNMI) RCM, one for the Canadian Centre for Climate
707 Modelling (CCCMA) RCM and one for the Danish Meteorological Institute (DMI) RCM).
708 These models were generated using change-factor downscaling approaches to model
709 spatial variation at local scales while correcting for differences between observed and
710 simulated baseline climates (see Platts et al.⁸⁷ for more details). We here concentrated
711 on one representative concentration pathway of the IPCC-AR5 (RCP 4.5) for the late
712 21st century (2071-2100, hereafter named 2085) and reconstructed the three SCGLR
713 selected CCs from the climatic predictions as follows: let $X_{rcp4.5}$ be the predicted future
714 climatic conditions. Let $m = \bar{X}$ and $S = sd(X)$ be the mean and standard deviation matrices
715 of the current climatic conditions. The predictive climatic components under future
716 scenarios are then equal to $f_{rcp4.5} = (X_{rcp4.5} - m)S\hat{u}$, where \hat{u} represents SCGLR CCs. We
717 then calculated the euclidean distance between the three current and the three
718 predicted CCs for each of the 18 models and then estimated the exposure to climate
719 change as the mean distance over the 18 models.

720 Adaptive capacity to climate change, $Adaptive_{clim}$, was assessed through the
721 phylogenetic diversity of predicted assemblages at the genus level. We used a recently
722 published dated phylogeny⁸⁸, covering 167 out of our 180 genera (representing 94% of
723 predicted individuals). We first tested if the studied taxa exhibited a significant
724 conservatism in their climate niches using Abouheif's permutation tests (Abouheif,
725 1999) on the taxa-specific score (γ) values on the three SCGLR climate components (γ
726 represents the influence of a CC on a given taxa distribution, see above). We then
727 measured the phylogenetic diversity (PD) of predicted assemblages at the genera level
728 using the Chao's PD index with an order q of 1 (equivalent to the Shannon index)⁸⁹ that
729 we used as a proxy of adaptive capacity.

730 Vulnerability to climate change, $Vulnerability_{clim}$, was finally estimated as the sum of
731 the three standardized (0 to 1) components:

$$732 \quad Vulnerability_{clim} = (Sensitivity_{clim}^{st} + Exposure_{clim}^{st} - Adaptive_{clim}^{st}).$$

733 $Vulnerability_{clim}$ theoretically ranges from -1 (low vulnerability) to 2 (high

734 vulnerability) and, due to the standardization of its three components, it expresses a
735 relative vulnerability over the study area and is thus little impacted by the IPCC scenario
736 chosen (RCP 4.5 or 8.5) because different scenarios predict different amplitudes of
737 changes but similar spatial patterns (Extended Data Fig. 7).

738 Forecasted human impact on forests in 2085 was assessed using our human-induced
739 forest disturbance intensity index combined with country-specific projections of human
740 populations in 2085. We assigned to each current town a country-specific relative
741 population increase drawn from the World population prospects (United Nations)⁹⁰ and
742 rebuild our index based on this modified dataset. This approach did not account for new
743 roads that may established by 2085, and thus tended to underestimate the increase in
744 anthropogenic pressure.

745 **Software and packages**

746 All analyses were performed and figures were created with the R statistical software⁹¹,
747 mostly using the ade4⁹², alphashape3d⁹³, ggplot2⁹⁴, raster⁹⁵, RgeoStat⁹⁶, entropart⁹⁷ and
748 SCGLR (<https://github.com/SCnext/SCGLR/>) packages. Data are archived in a public
749 repository⁹⁸.

750 **Data availability**

751 All maps and data used for this article are accessible online in a public repository at
752 <http://dx.doi.org/10.18167/DVN1/UCNCA7>. Raw floristic data are, however, archived in
753 a private data repository, due to the highly sensitive nature of commercial inventory
754 data, and access may be granted for research purpose using the form provided in the
755 public repository.

756 **Code availability**

757 R scripts are available at <https://github.com/MaximeRM/ScriptNature>.

758 **Methods references**

- 759 51. Réjou-Méchain, M. *et al.* Detecting large-scale diversity patterns in tropical trees:
760 Can we trust commercial forest inventories? *Forest Ecology and Management* **261**,
761 187–194 (2011).
- 762 52. Chase, M. W. *et al.* An update of the Angiosperm Phylogeny Group classification for
763 the orders and families of flowering plants: APG III. *Botanical Journal of the Linnean*
764 *Society* **161**, 105–121 (2009).
- 765 53. Dauby, G. *et al.* RAINBIO: A mega-database of tropical African vascular plants
766 distributions. *PhytoKeys* 1 (2016).
- 767 54. African Plant Database (version 3.4.0). Conservatoire et Jardin botaniques de la
768 Ville de Genève and South African National Biodiversity Institute, Pretoria. Retrieved the
769 10/02/2017.
- 770 55. Chave, J. *et al.* Towards a worldwide wood economics spectrum. *Ecology Letters*
771 **12**, 351–366 (2009).
- 772 56. Zanne, A. E. *et al.* Global wood density database. *Dryad*. Identifier: [http://hdl.](http://hdl.handle.net/10255/dryad)
773 [handle.net/10255/dryad](http://hdl.handle.net/10255/dryad) **235**, (2009).
- 774 57. Gourlet-Fleury, S. *et al.* Environmental filtering of dense-wooded species controls
775 above-ground biomass stored in African moist forests. *Journal of Ecology* **99**, 981–990
776 (2011).
- 777 58. Westoby, M. & Wright, I. J. Land-plant ecology on the basis of functional traits.
778 *Trends in Ecology & Evolution* **21**, 261–268 (2006).
- 779 59. Chave, J. *et al.* Improved allometric models to estimate the aboveground biomass of
780 tropical trees. *Global Change Biology* **20**, 3177–3190 (2014).
- 781 60. Bénédet, F. *et al.* CoForTraits, African plant traits information database . Version
782 1.0. (2013).

- 783 61. Davies, T. J. *et al.* Phylogenetic conservatism in plant phenology. *Journal of ecology*
784 **101**, 1520–1530 (2013).
- 785 62. Cramer, W. *et al.* Global response of terrestrial ecosystem structure and function to
786 CO₂ and climate change: Results from six dynamic global vegetation models. *Global*
787 *change biology* **7**, 357–373 (2001).
- 788 63. Menzel, A. Phenology: Its importance to the global change community. *Climatic*
789 *change* **54**, 379 (2002).
- 790 64. Borchert, R., Rivera, G. & Hagnauer, W. Modification of Vegetative Phenology in a
791 Tropical Semi-deciduous Forest by Abnormal Drought and Rain 1. *Biotropica* **34**, 27–39
792 (2002).
- 793 65. Kraft, N. J. B., Valencia, R. & Ackerly, D. D. Functional traits and niche-based tree
794 community assembly in an amazonian forest. *Science* **322**, 580–582 (2008).
- 795 66. Schamp, B. S. & Aarssen, L. W. The assembly of forest communities according to
796 maximum species height along resource and disturbance gradients. *Oikos* **118**, 564–
797 572 (2009).
- 798 67. New, M., Lister, D., Hulme, M. & Makin, I. A high-resolution data set of surface
799 climate over global land areas. *Climate research* **21**, 1–25 (2002).
- 800 68. Hijmans, R. J., Cameron, S. E., Parra, J. L., Jones, P. G. & Jarvis, A. Very high
801 resolution interpolated climate surface for global land areas. *International journal of*
802 *climatology* **25**, 1965–1978 (2005).
- 803 69. Funk, C. *et al.* The climate hazards infrared precipitation with stations—a new
804 environmental record for monitoring extremes. *Scientific data* **2**, 150066 (2015).
- 805 70. Nachtergaele, F. *et al.* The harmonized world soil database. in *Proceedings of the*
806 *19th World Congress of Soil Science, Soil Solutions for a Changing World, Brisbane,*
807 *Australia, 1-6 August 2010* 34–37 (2010).

- 808 71. Woolmer, G. *et al.* Rescaling the human footprint: A tool for conservation planning at
809 an ecoregional scale. *Landscape and Urban Planning* **87**, 42–53 (2008).
- 810 72. Venter, O. *et al.* Sixteen years of change in the global terrestrial human footprint and
811 implications for biodiversity conservation. *Nature Communications* **7**, 12558 (2016).
- 812 73. Geldmann, J., Joppa, L. N. & Burgess, N. D. Mapping change in human pressure
813 globally on land and within protected areas. *Conservation biology* **28**, 1604–1616
814 (2014).
- 815 74. Linard, C., Gilbert, M., Snow, R. W., Noor, A. M. & Tatem, A. J. Population
816 distribution, settlement patterns and accessibility across Africa in 2010. *PloS one* **7**,
817 e31743 (2012).
- 818 75. Lloyd, C. T. *et al.* Global spatio-temporally harmonised datasets for producing high-
819 resolution gridded population distribution datasets. *Big Earth Data* **3**, 108–139 (2019).
- 820 76. Boulesteix, A.-L. & Strimmer, K. Partial least squares: A versatile tool for the
821 analysis of high-dimensional genomic data. *Briefings in bioinformatics* **8**, 32–44 (2007).
- 822 77. Carrascal, L. M., Galván, I. & Gordo, O. Partial least squares regression as an
823 alternative to current regression methods used in ecology. *Oikos* **118**, 681–690 (2009).
- 824 78. Tenenhaus, M. *La régression PLS: Théorie et pratique*. (Editions Technip, 1998).
- 825 79. Sabatier, R., Lebreton, J. D. & Chessel, D. Principal component analysis with
826 instrumental variables as a tool for modelling composition data. *Multiway data analysis*
827 341–352 (1989).
- 828 80. Ter Braak, C. J. The analysis of vegetation-environment relationships by canonical
829 correspondence analysis. in *Theory and models in vegetation science* 69–77 (Springer,
830 1987).
- 831 81. Bry, X. & Verron, T. THEME: THEmatic model exploration through multiple co-
832 structure maximization. *Journal of Chemometrics* **29**, 637–647 (2015).

- 833 82. Cornu, G., Mortier, F., Trottier, C. & Bry, X. SCGLR: Supervised Component
834 Generalized Linear Regression. (2016).
- 835 83. Ward Jr, J. H. Hierarchical grouping to optimize an objective function. *Journal of the*
836 *American statistical association* **58**, 236–244 (1963).
- 837 84. Scrucca, L., Fop, M., Murphy, T. B. & Raftery, A. E. Mclust 5: Clustering,
838 classification and density estimation using gaussian finite mixture models. *The R journal*
839 **8**, 289 (2016).
- 840 85. Dormann, C. F. *et al.* Methods to account for spatial autocorrelation in the analysis
841 of species distributional data: A review. *Ecography* **30**, 609–628 (2007).
- 842 86. Renard, D. *et al.* RGeostats: The Geostatistical package 11.0. 1. *MINES ParisTech*
843 (2014).
- 844 87. Platts, P. J., Omeny, P. A. & Marchant, R. AFRICLIM: High-resolution climate
845 projections for ecological applications in Africa. *African Journal of Ecology* **53**, 103–108
846 (2015).
- 847 88. Janssens, S. B. *et al.* A large-scale species level dated angiosperm phylogeny for
848 evolutionary and ecological analyses. *Biodiversity data journal* **8**, (2020).
- 849 89. Chao, A., Chiu, C.-H. & Jost, L. Phylogenetic diversity measures based on Hill
850 numbers. *Philosophical Transactions of the Royal Society B: Biological Sciences* **365**,
851 3599–3609 (2010).
- 852 90. Nations, U. World population prospects: The 2017 revision, key findings and
853 advance tables. *United Nations, New york* (2017).
- 854 91. R Core Team. *R: A language and environment for statistical computing*. (R
855 Foundation for Statistical Computing, 2017).
- 856 92. Chessel, D., Dufour, A. B. & Thioulouse, J. The ade4 package-I- One-table
857 methods. *R News* **7**, 47–52 (2004).

- 858 93. Lafarge, T. & Pateiro-Lopez, B. *Alphashape3d: Implementation of the 3D alpha-*
859 *shape for the reconstruction of 3D sets from a point cloud.* (2017).
- 860 94. Wickham, H. *Ggplot2: Elegant graphics for data analysis.* (Springer-Verlag New
861 York, 2016).
- 862 95. Hijmans, R. J. *Raster: Geographic data analysis and modeling.* (2017).
- 863 96. Renard, D. *et al. RGeostats: Geostatistical package.* (2017).
- 864 97. Marcon, E. & Hérault, B. entropart: An R package to measure and partition diversity.
865 *Journal of Statistical Software* **67**, 1–26 (2015).
- 866 98. Réjou-Méchain, M. *et al. Maps of central African rainforest composition and*
867 *vulnerability*, doi:10.18167/DVN1/UCNCA7, CIRAD Dataverse, V2, (2021).

868

869

870 **Acknowledgements**

871 We thank the 105 forest companies that provided access, albeit restricted, to their
872 inventory data for research purposes and members of the central african plot network
873 (<https://central-african-plot-network.netlify.app/>), Y. Yalibanda, F. Allah-Barem, F. Baya,
874 F. Boyemba, M. Mbasi Mbula, P. Berenger, M. Mazengue, V. Istace, I. Zombo, E. Forni,
875 Nature+ and the CEB-Precious Woods company for giving access to the scientific
876 inventories described in Fig. S4, some of which were funded by the AFD and the FFEM
877 (e.g. DynAfFor and P3FAC projects). We thank J. Chave, P. Couteron, S. Lewis and M.
878 Tadesse for their helpful comments and discussions on previous versions. We also
879 thank the five reviewers for their highly constructive comments on previous versions, B.
880 Sultan for useful discussions on climate projections, O.J. Hardy for advices on
881 phylogenetical analyses, B. Locatelli for advices on vulnerability analyses, G. Vieilledent
882 for our discussions on the human-induced forest disturbance intensity index and A.
883 Stokes for English editing. This work was supported by the CoForTips project (ANR-12-

884 EBID-0002) funded by the ERA-NET BiodivERsA, with the national funders ANR,
885 BELSPO and FWF, as part of the 2012 BiodivERsA call for research proposals, the
886 GAMBAS project funded by the French National Research Agency (ANR-18-CE02-
887 0025) and the project 3DForMod funded by the UE FACCE ERA-GAS consortium
888 (ANR-17-EGAS-0002-01). This study is a contribution to the research program of LMI
889 DYCOFAC (Dynamique des écosystèmes continentaux d’Afrique Centrale en contexte
890 de changements globaux).

891 **Author contributions,**

892 Conceptualization: M.R-M., F.M., R.P. & S.G-F; data curation: G.C. & F.B.; formal
893 analysis: M.R-M. & F.M.; project administration: C.G.; writing – original draft: M.R-M.,
894 F.M., R.P. & S.G-F; writing – review & editing: all authors.

895 **Competing interests**

896 Authors declare no competing interests.

897 **Supplementary Information** is available for this paper

898 **Correspondence and requests for materials should be addressed to**

899 maxime.rejou@ird.fr

900 **Reprints and permissions information is available at www.nature.com/reprints**

901

902

903 **Extended data figure/table legends:**

Group	Name	Main families	Representative taxa	Area	PA	Logging	Phum	CC1	CC2	CC3
1	Atlantic highland evergreen	Fabaceae (19%), Burseraceae (17%), Myristicaceae (13%)	Anisophyllea spp., Baillonella toxisperma, Aucoumea klaineana, Bobgunnia fistuloides, Testulea gabonensis	79,400	9	70	0.48	-3.4	3.4	-1.1
2	Atlantic coastal evergreen	Fabaceae (27%), Burseraceae (17%), Myristicaceae (15%)	Anthostema aubryanum, Scyttopetalum klaineum, Calpocalyx spp., Coula edulis, Tetraberlinia bifoliolata	17,700	54	36	0.35	-5.2	0.1	4.6
3	Atlantic inland evergreen	Fabaceae (27%), Burseraceae (15%), Myristicaceae (14%)	Calpocalyx spp., Letestua durissima, Eurypetalum spp., Coula edulis, Tetraberlinia bifoliolata	60,800	22	69	0.35	-3.8	-0.1	3.0
4	Margin semideciduous	Malvaceae (16%), Fabaceae (13%), Cannabaceae (11%)	Aubrevillea kerstingii, Holoptelea grandis, Mansonia altissima, Trilepisium madagascariense, Morus mesozygia	87,600	4	20	0.42	4.1	2.4	2.0
5	Evergreen-semideciduous on sandstone	Fabaceae (15%), Sapotaceae (15%), Annonaceae (9%)	Manilkara spp., Oldfieldia africana, Balanites wilsoniana, Aufranella congolensis, Synsepalum spp.	22,200	23	80	0.27	3.2	2.0	1.0
6	Semideciduous	Fabaceae (20%), Annonaceae (10%), Malvaceae (8%)	Pericopsis elata, Fernandoa adolfi friderici, Dasylepis seretii, Desplatsia spp., Entandrophragma cylindricum	206,400	10	34	0.26	2.6	-0.3	-0.2
7	Central evergreen	Fabaceae (33%), Annonaceae (9%), Olacaceae (9%)	Millettia spp., Brachystegia spp., Ochna spp., Gilbertiodendron dewevrei, Rothmannia spp.	265,900	23	9	0.22	0.6	-3.8	-2.3
8	Mixed evergreen	Fabaceae (30%), Olacaceae (10%), Myristicaceae (8%)	Diogoa zenkeri, Elaeis guineensis, Cryptosepalum spp., Bikinia spp., Ochthocosmus spp.	158,200	10	45	0.40	-1.4	-2.2	-0.2
9	Degraded semideciduous	Fabaceae (14%), Cannabaceae (13%), Urticaceae (8%)	Pseudospondias spp., Musanga cecropioides, Pterygota spp., Ricinodendron heudelotii, Afzelia spp.	40,000	10	6	0.73	1.1	2.0	1.6
10	Semideciduous-evergreen transition	Fabaceae (22%), Annonaceae (10%), Olacaceae (8%)	Uapaca spp., Musanga cecropioides, Annickia spp., Croton spp., Pseudospondias spp.	180,000	15	29	0.37	0.4	-0.3	-1.5

904

905 **Extended Data Table 1 | Characteristics of the floristic groups.** For each floristic
 906 group information is given on the three most abundant families (APGIII classification,
 907 except for the subfamilies Caesalpiniaceae and Mimosaceae, which were considered
 908 here independently due to their different ecological strategies), the five most
 909 representative taxa (i.e., taxa having the highest A score of the Dufrêne and Legendre
 910 index), the total area (km²) covered by each group, the percentage of the area
 911 covered by protected areas (PA) and dedicated to logging activities (Logging), the mean
 912 probability of being impacted by human activities (phum, this study) and the mean value
 913 of the three climatic components (CCs) that best explain the current distribution of
 914 central African trees (this study).

915

CODE	Description	Mean (range)	CC1	CC2	CC3
C1	Annual Mean Temperature (°C)	24.7 (22.7 - 26.4)	-0.01	-0.54	0.43
C2	Mean Diurnal Range (°C)	9.4 (6.2 - 11)	0.88	0.01	0
C3	Isothermality (C2/C7) (* 100) (unitless)	76.6 (53.1 - 89.8)	-0.06	-0.67	-0.16
C4	Temperature Seasonality (Coefficient of Variation of kelvin values) (%)	1.5 (0.7 - 3.6)	-0.21	0.54	0.08
C5	Max Temperature of Warmest Month (°C)	31.1 (28.6 - 33.9)	0.38	-0.03	0.51
C6	Min Temperature of Coldest Month (°C)	18.8 (16.5 - 22)	-0.15	-0.76	0.06
C7	Temperature Annual Range (C5-C6) (°C)	12.3 (9.4 - 16)	0.53	0.32	0.1
C8	Mean Temperature of Wettest Quarter (°C)	24.5 (22 - 26.6)	-0.21	-0.42	0.27
C9	Mean Temperature of Driest Quarter (°C)	24.2 (20.9 - 27.2)	0.3	-0.53	0.13
C10	Mean Temperature of Warmest Quarter (°C)	25.6 (23.9 - 27.3)	-0.01	-0.19	0.75
C11	Mean Temperature of Coldest Quarter (°C)	23.8 (20.5 - 25.5)	0.08	-0.73	0.14
C12	Annual Precipitation (mm)	1733.5 (1219.7 - 2983)	-0.26	-0.06	0.06
C13	Precipitation of Wettest Month (mm)	263.2 (195.7 - 608.7)	-0.43	0.05	0.11
C14	Precipitation of Driest Month (mm)	31.9 (0 - 112.4)	0.2	-0.4	-0.16
C15	Precipitation Seasonality (Coefficient of Variation) (%)	52.1 (21.7 - 84.5)	-0.29	0.51	0.15
C16	Precipitation of Wettest Quarter (mm)	665 (435.8 - 1273.7)	-0.28	0.01	0.15
C17	Precipitation of Driest Quarter (mm)	137.7 (2 - 405.2)	0.14	-0.53	-0.13
C18	Precipitation of Warmest Quarter (mm)	434.3 (220.7 - 816.1)	-0.9	0	0
C19	Precipitation of Coldest Quarter (mm)	302.8 (0.7 - 1332.9)	0.8	0	0.02
meanET0	mean monthly evapotranspiration ¹ (mm)	133.8 (109.9 - 146.6)	0.76	-0.1	0.02
meanCWB	mean climatic water balance ² (mm)	10.6 (-19.2 - 134.3)	-0.52	0.01	0.02
sumCWD	total climatic water deficit ³ (mm)	-1617.8 (-4466.3 - -55.8)	-0.59	-0.29	-0.07
maxCWD	maximum cumulative water deficit ⁴ (mm)	-299.3 (-596 - -21.9)	-0.08	-0.6	-0.21
MCWD	maximum climatic water deficit ⁵ (mm)	-312.3 (-596 - -37.7)	-0.08	-0.62	-0.18

¹ meanET0 was calculated using the Hargreaves formula with $meanET0 = \frac{1}{n} \sum_{i=1}^n ET0_i$ where $ET0_i$ is the evapotranspiration of month i calculated as $ET0_i = 0.0023 * 0.408RA_i * (Tavg_i + 17.8) * TD_i^{0.5}$ with RA the mean extrasolar radiation of month i in $MJ m^{-2} d^{-1}$, $Tavg_i$ the average daily temperature of month i in (°C), computed as the average of the mean maximum and minimum temperature of month i and TD_i the mean temperature range of month i in (°C), computed as the difference between mean maximum and minimum temperature of month i .

² $meanCWB = \frac{1}{n} \sum_{i=1}^n P_i - ET0_i$ where P_i is the precipitation of month i .

^{3,4} $sumCWD = \sum_{i=1}^n CWD_i$ and $maxCWD = max(CWD_i)$ where $CWD_i = sum_{j=1}^i WD_j$ with $WD_i = WD_{i-1} + P_i - ET0_i$ if $WD_{i-1} + P_i - ET0_i < 0$ or $WD_i = 0$ if $WD_{i-1} + P_i - ET0_i \geq 0$. To compute CWD_i , the wettest month was set as $i=1$ at the grid cell level.

⁵ $MCWD = sum_{i=1}^n min(0, P_i - ET0_i)$.

916

917 **Extended Data Table 2 | Climatic predictors.** Correlations with the three climatic
918 components (CCs) are given in the last three columns (see also Extended Data Fig. 4).

919 ¹meanET0 was calculated using the Hargreaves formula with $meanET0 = \frac{1}{n} \sum_{i=1}^n ET0_i$

920 where $ET0_i$ is the evapotranspiration of month i calculated as $ET0_i = 0.0023 * 0.408RA_i * (Tavg_i + 17.8) * TD_i^{0.5}$ with RA_i the mean extrasolar radiation of month i in $MJ m^{-2} d^{-1}$,

921 $Tavg_i$ the average daily temperature of month i in °C, computed as the average of the
922 mean maximum and minimum temperature of month i , and TD_i the mean temperature
923 range of month i in °C, computed as the difference between mean maximum and
924 minimum temperature of month i .

925 ² $meanCWB = \frac{1}{n} \sum_{i=1}^n P_i - ET0_i$ where P_i is the precipitation

926 of month i .^{3,4} $sumCWD = \sum_{i=1}^n CWD_i$ and $maxCWD = \max(CWD_i)$ where $sumCWB = \sum_{i=1}^n CWD_i$

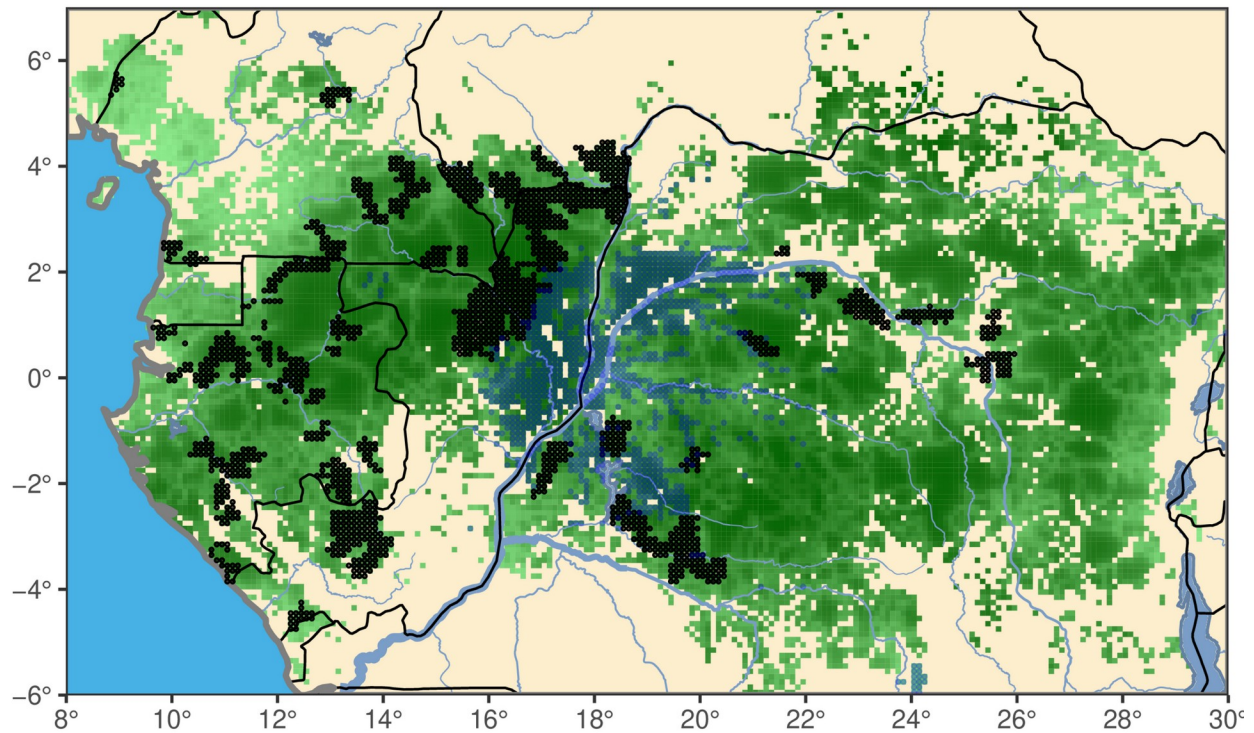
927 with $WD_i = WD_{i-1} + P_i - ET 0_i$ if $WD_i = WD_{i-1} + P_i - ET 0_i$ or $WD_i = 0$ if $(WD_{i-1} + P_i - ET 0_i) \geq 0$. To

928 compute CWD_i , the wettest month was set as $i=1$ at the grid cell level.⁵

929 $MCWD = \sum_{i=1}^n \min(0, P_i - ET 0_i)$.

930

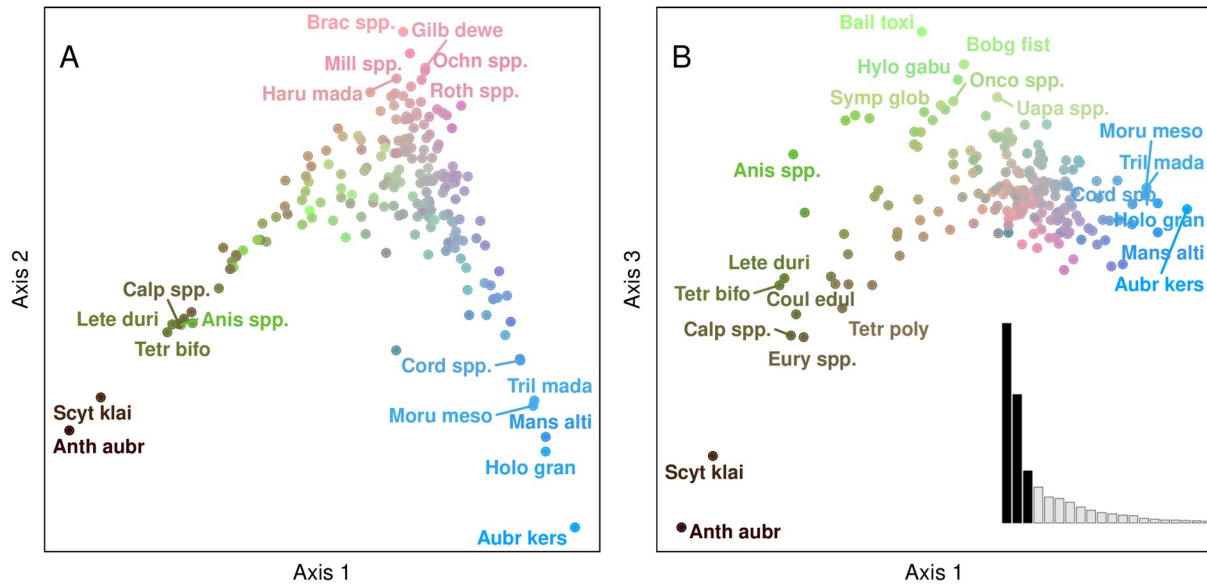
931



932

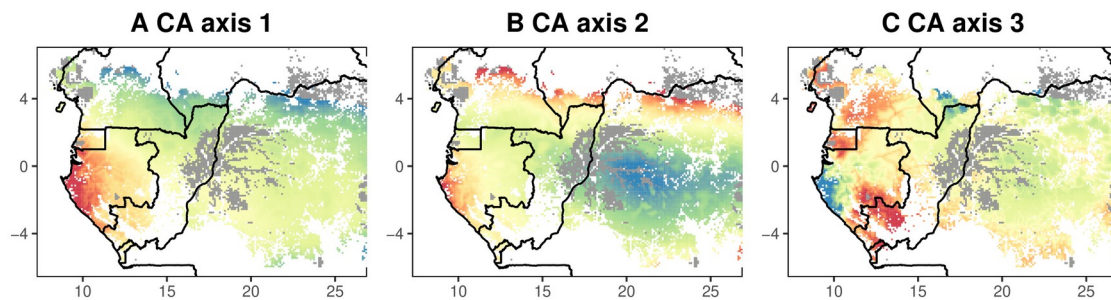
933 **Extended Data Figure 1 | Study area and sampling plots.** In green, the current
934 distribution of tropical forests following the European Space Agency Climate Change
935 Initiative (ESA-CCI) landcover (V.1.6) with a dark green-to-white gradient representing
936 anthropogenic pressure (see methods) and non-forested areas represented in beige;
937 the sampling grid cells ($n=1,571$ 10×10 -km² grid cells) are in black and the flooding
938 forests, as proposed by the ESA-CCI landcover, are in blue.

939



940

941 **Extended Data Figure 2 | Taxon CA planes 1-2 (A) and 1-3 (B) with labels for the**
 942 **12 most representative taxa on each axis.** Color code corresponds to that reported
 943 in Fig. 1. The first eigenvalues are reported in the B panel, highlighting in black the first
 944 three axes. Taxon codes and scores of the 193 taxa are given in Table S2.

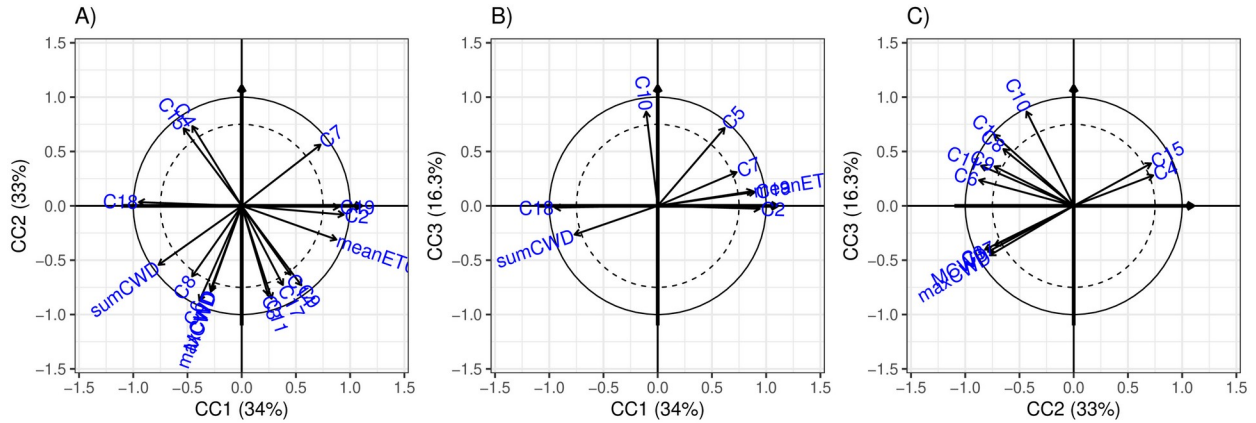


945

946 **Extended Data Figure 3 | Individual predicted floristic gradients illustrated by the**
 947 **three first axes of the correspondence analysis (CA) performed on predicted**
 948 **taxon abundances.** A composite map of these three axes is given in Fig. 1 and the
 949 corresponding taxon CA planes are provided in Extended Data Fig. 2.

950

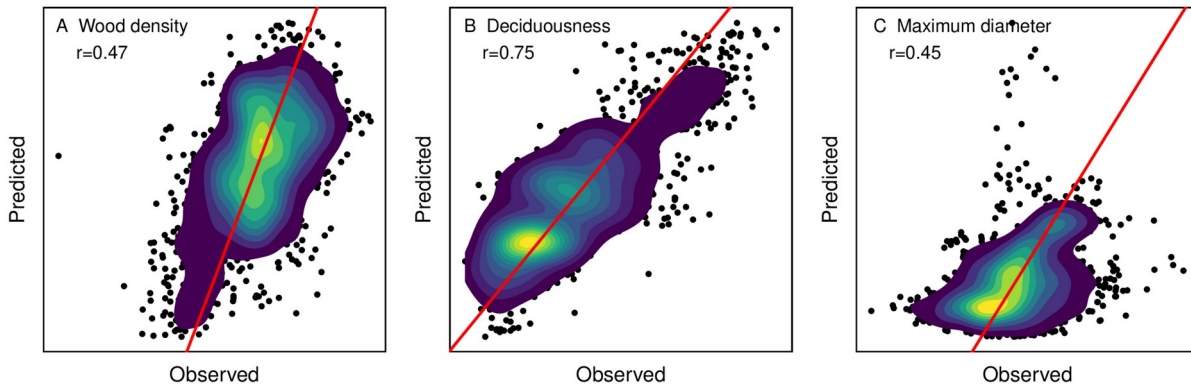
951



952 **Extended Data Figure 4 | Plans 1-2 (A), 1-3 (B) and 2-3 (C) of the SCGLR climatic**
953 **components (CCs).** All climatic variables having a correlation < 0.75 with the two
954 components (dashed circle) were excluded for the sake of clarity. For abbreviations, see
955 Extended Data Table 2.

956

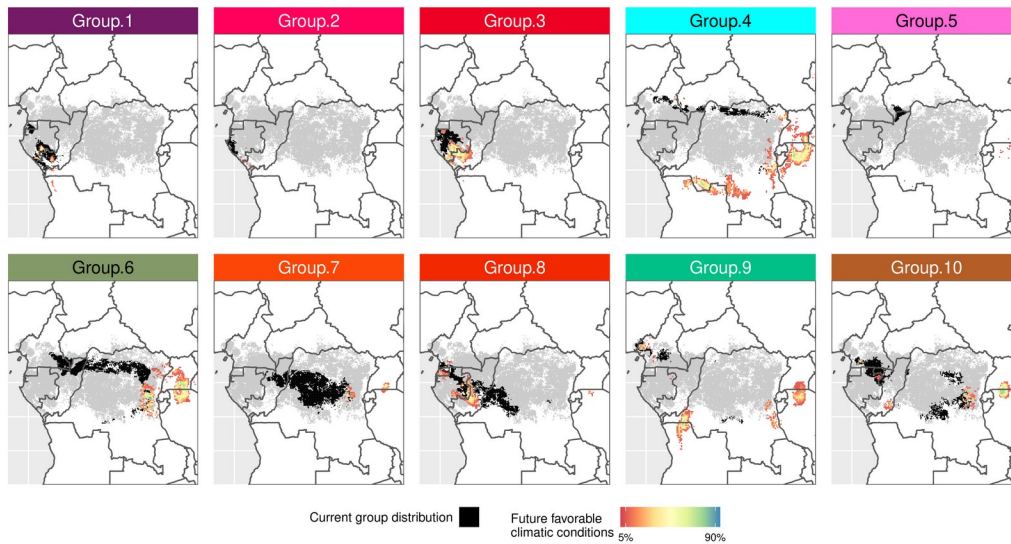
957



958

959 **Extended Data Figure 5 | Spatial cross-validation results of the predictions of**
960 **functional assemblages.** The observed and predicted community weighted mean trait
961 values within the 1,571 10x10-km² grid cells are given for (A) wood density; (B)
962 deciduousness and (C) maximum diameter. The 1:1 line is displayed in red.

963



964

965 **Extended Data Figure 6 | Projected changes under RCP scenario 4.5 in 2085 of**
 966 **the climatic conditions of the ten forest types.** Areas where climate models predict
 967 similar climatic components (CCs) values as those currently found within forest types (in
 968 black) are illustrated with a color gradient indicating the level of agreement amongst the
 969 18 climate models (in %; no color indicates that none of the original 18 climate models
 970 predicted similar conditions). More specifically, we used 3D concave hull (alpha shape)
 971 models to assess where the combinations of current Ccs corresponding to each forest
 972 type are predicted to be represented in 2085.

973

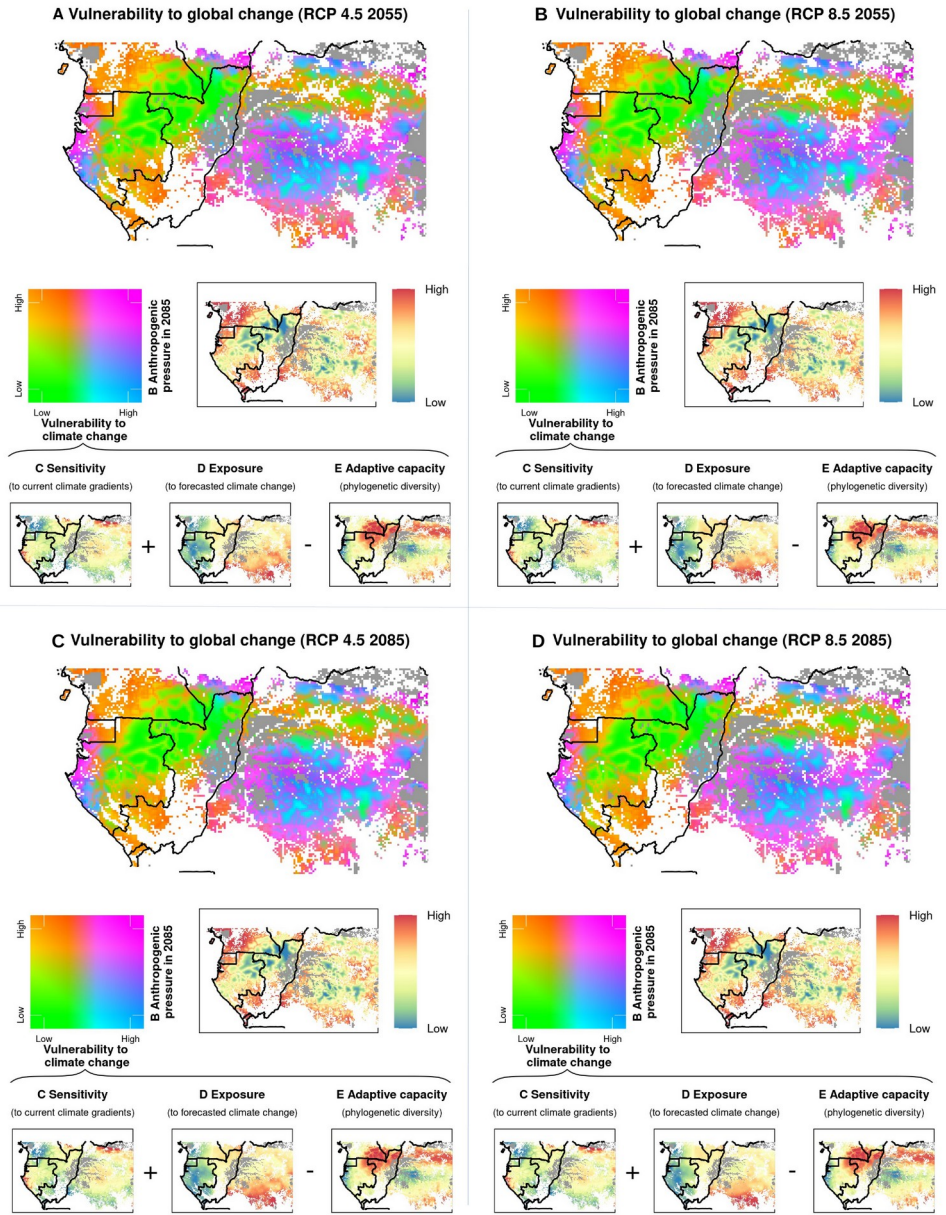
974

975

976

977

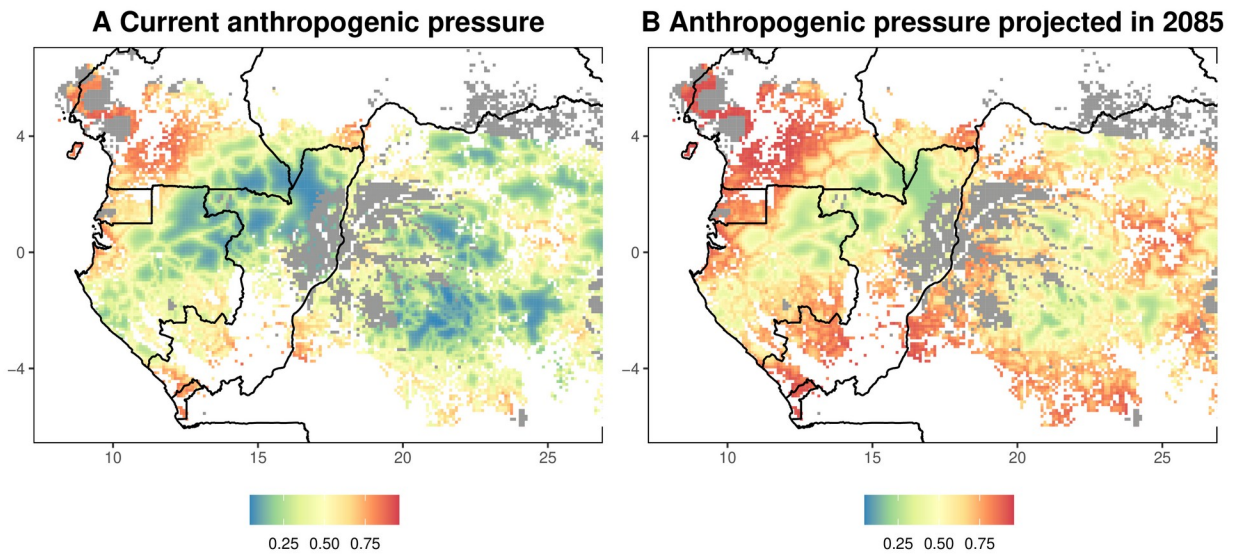
978



979

980 **Extended Data Figure 7 | The vulnerability map under two different RCP**
 981 **scenarios, RCP 4.5 and RCP 8.5, and for two years, year 2055 and year 2085. As**
 982 **can be seen, the predicted vulnerability is little impacted by the IPCC scenario chosen**
 983 **because it expresses a relative vulnerability over the study area and, if different**
 984 **scenarios predict different amplitudes of climate change, spatial patterns of climate**
 985 **exposure remains similar (see Methods).**

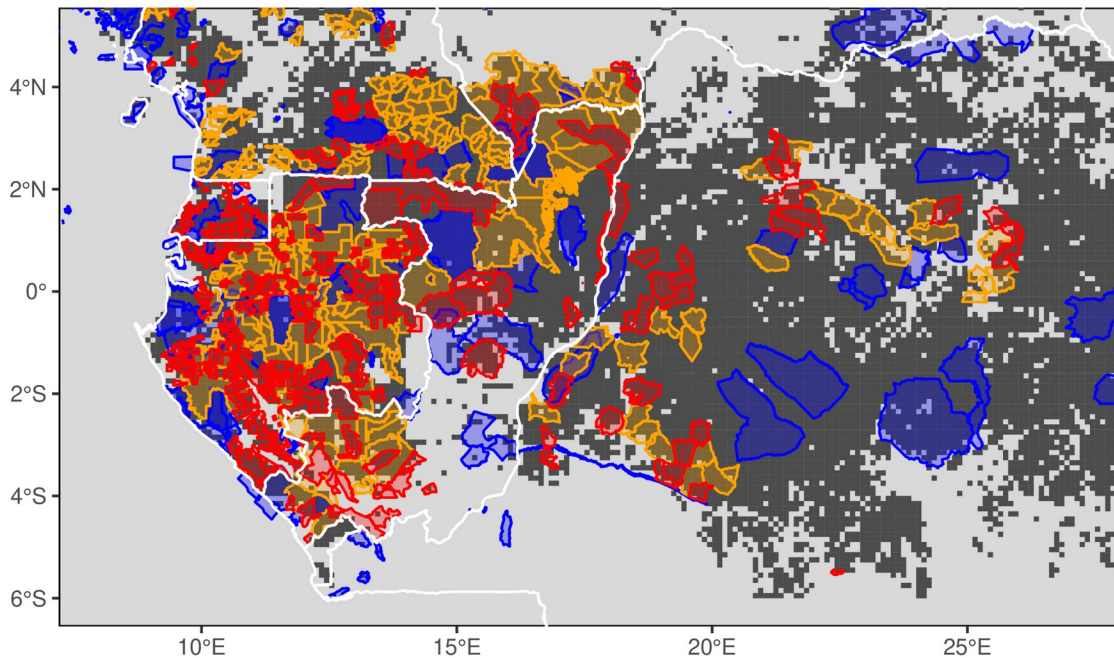
986



987

988 **Extended Data Figure 8 | Current and projected anthropogenic pressure over**
989 **central Africa predicted from our index of human-induced forest disturbance**
990 **intensity.**

991



993

994 **Extended Data Figure 9 | Protected area network (blue) and areas dedicated to**995 **logging activities (orange and red) in central Africa.** Data on protected areas were

996 obtained from the World Database on Protected Areas (last access: 14/08/2018)

997 excluding marine, hunting and game-oriented areas except for the Democratic Republic

998 of Congo where data from the World Resource Institute were used and downloaded

999 from ArcGIS hub (last access: 01/06/2019). Logging activity data were kindly provided

1000 by the Observatoire des Forêts d'Afrique Centrale based on an unpublished work

1001 completed in June 2018, except for DRC where more updated data (June 2019) were

1002 provided by the AGEDUFOR national project. Areas in orange illustrate forest

1003 concessions that are known to have, or to be in the process of having, an officially

1004 validated sustainable forest management plan. Red areas illustrate forest areas that are

1005 currently dedicated to logging but that either do not have an official management plan or

1006 have an uncertain status.